nature climate change

Article

https://doi.org/10.1038/s41558-025-02273-6

Drought legacies delay spring green-up in northern ecosystems

Received: 3 August 2024

Accepted: 5 February 2025

Published online: 20 March 2025

Check for updates

Ying Liu[1], Yao Zhang[1] ✉, Josep Peñuelas[2,3], Steven A. Kannenberg[4], Haibo Gong[1], Wenping Yuan[1], Chaoyang Wu[5], Sha Zhou[6] & Shilong Piao[1]

Global warming has increased the frequency and intensity of droughts, causing large impacts on the structure and functioning of terrestrial ecosystems. The direct effect of droughts on autumn senescence is well-documented, but the extent to which the legacy effects influence plant phenology of the following year remains unclear. Using satellite greenness data and long-term in situ observations, we demonstrate that droughts substantially delay the green-up and leaf unfolding of the next spring, particularly following prolonged events with delayed soil moisture recovery. These delays cannot be explained by state-of-the-art phenology models and are strongly linked to postdrought temperature, local climate, drought characteristics and reductions in photosynthesis. Compared to the endogenous memory effects within plants themselves, the exogenous memory effects through changes in environment are five times stronger in drylands and twice as strong in non-drylands. Given projections of increased drought frequency and severity, future advances in spring phenology may be less pronounced than previously anticipated.

Advances of biological spring, such as leaf unfolding or green-up, have been globally recorded based on in situ and remotely sensed observations over recent decades[1–4]. An earlier start of the growing season (SOS) enhances photosynthesis and spring carbon uptake[5–7], warms the atmosphere[8] and potentially alters plant–animal interactions[9]. Recent insights into ecological memory, the antecedent events with downstream consequences, highlight strong legacy impacts of SOS on autumn leaf senescence through both endogenous memory effects, such as fixed leaf lifespan and carbon sink limitation[10–12], and exogenous memory effects, such as soil moisture stress from enhanced early-season transpiration[13,14]. Given its profound implications, recent studies strive for accurate projections of future SOS changes.

It has been widely accepted that preseason warming is the primary factor contributing to SOS advancement[15]. State-of-the-art spring phenology models also incorporate winter temperature to quantify chilling requirements and radiation for photoperiod regulation[16,17], partially explaining reduced temperature sensitivity observed in spring leaf unfolding over recent decades[18,19]. Recent studies indicate that memory effects from the preceding year may strongly regulate SOS. For instance, greater carbon uptake in the previous year can lead to advanced spring leaf unfolding[20]. However, understanding of these memory effects remains limited, particularly regarding how drought, known for its strong legacy effects on plant growth, influences the next spring green-up[21,22]. As drought frequency and intensity are projected to increase with future warming[23], which may be further exacerbated by increased evapotranspiration alongside vegetation greening[14,24], the lack of a mechanistic understanding of drought legacies may introduce substantial uncertainty into future spring phenology projections.

One major challenge hindering the accurate quantification of drought legacy effects is their dual nature as both endogenous and exogenous. Persistent drought may deplete non-structural carbon

[1]Institute of Carbon Neutrality, Sino-French Institute for Earth System Science, College of Urban and Environmental Sciences, Peking University, Beijing, China. [2]CREAF, Barcelona, Spain. [3]CSIC, Global Ecology Unit CREAF-CSIC-UAB, Barcelona, Spain. [4]Department of Biology, West Virginia University, Morgantown, WV, USA. [5]Institute of Geographic Sciences and Natural Resources Research, Chinese Academy of Sciences, Beijing, China. [6]Faculty of Geographical Science, Beijing Normal University, Beijing, China. ✉e-mail: zhangyao@pku.edu.cn

https://doi.org/10.1038/s41558-025-02273-6

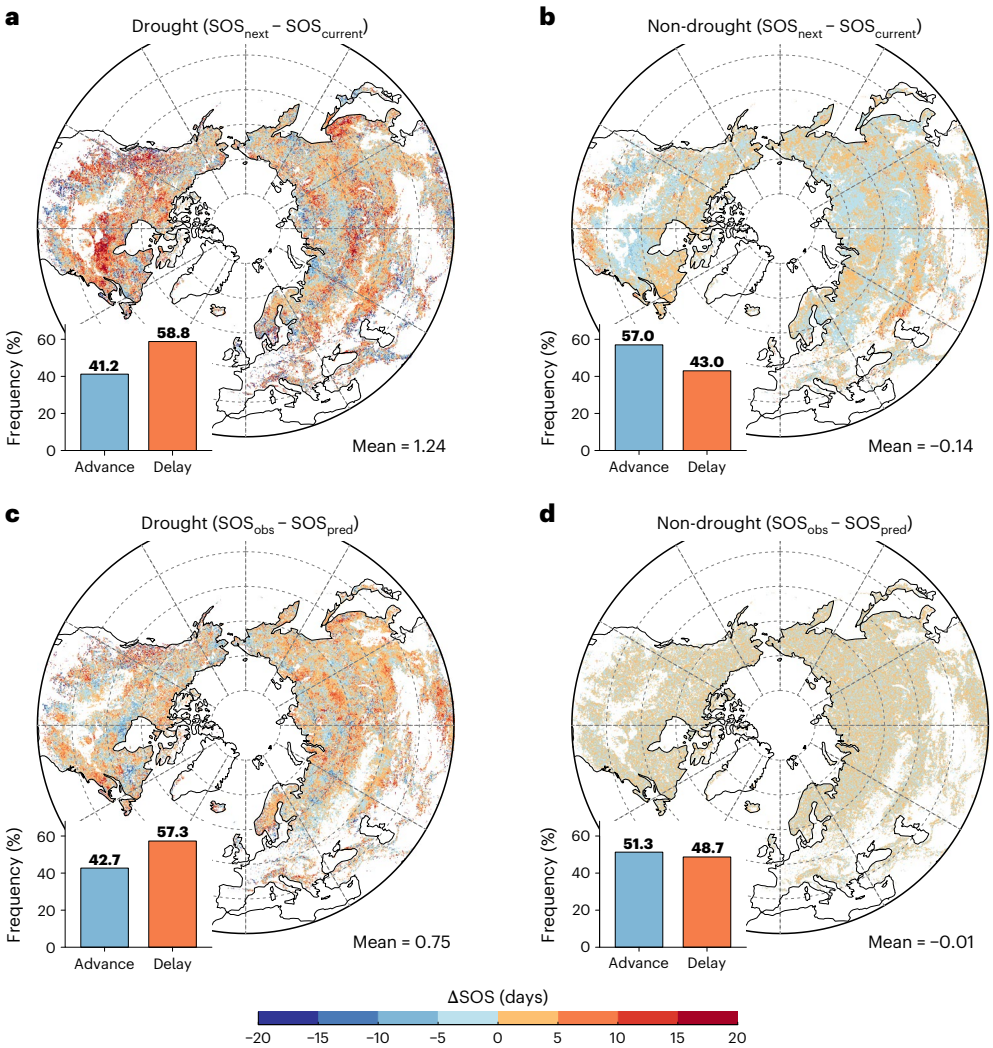

Fig. 1 | Effects of drought on the SOS of the next year from GIMMS NDVI 3g dataset. a–d, Spatial distribution of mean changes between SOS_{next} and $SOS_{current}$ after drought (**a**) and non-drought (**b**) years, and differences between SOS_{obs} and SOS_{pred} after drought (**c**) and non-drought (**d**) years. Insets show proportion of area with SOS delayed (orange) or advanced (blue) by drought.

and impede nutrient recycling, both factors (endogenous) that can delay spring leaf unfolding[25]. If soil moisture (SM) fails to fully recover even after spring begins, this carryover water stress (exogenous) may also inhibit vegetation green-up[26,27]. Moreover, these effects may be further confounded by warming or cooling effects induced by SM deficits through complex land–atmosphere interactions[28]. However, differentiating endogenous and exogenous drought legacy effects is challenging at broad spatial and temporal scales. To distinguish between the endogenous and exogenous effects, while accounting for warming effects, we categorized drought events into three types on the basis of whether SM recovered within the same growing season as drought occurrence or before or after the onset of the next spring (Methods; Extended Data Fig. 1). Drought events were identified by considering both the water deficit and its impact on terrestrial ecosystems. Specifically, we used SM and deseasonalized vegetation index and identified droughts when both fell below 0.5 s.d. for at least two consecutive months (Methods; Extended Data Fig. 1). Using long-term satellite observations (global inventory modelling and mapping studies (GIMMS) NDVI 3g, 1982–2015) and ground phenological records (Pan European phenology network (PEP725) (1945–2016), Russian 'chronicles of nature' network (RCNN) (1901–2017) and China phenological observation network (CPON) (1963–2014)), together with state-of-the-art phenology models, we investigated the impact of drought events on the green-up of the subsequent year across mid- and high-latitudinal Northern Hemisphere.

Legacy effect of drought events on spring phenology

To assess the legacy effect of drought on the SOS of the subsequent year, we calculated the difference in satellite-derived SOS (ΔSOS) for the drought year compared to the year following (observation-based method). SOS is defined as the date when the normalized difference vegetation index (NDVI) first surpasses 20% of its annual amplitude (Supplementary Fig. 1). Since droughts mostly happen after SOS, positive and negative values of ΔSOS (SOS_{next} – $SOS_{current}$) indicate delayed and advanced SOS induced by drought legacies, respectively. As a reference, we also calculated ΔSOS for years without drought in a similar way. This observation-based method shows that after droughts, 58.8% of the pixels experience delayed SOS_{next} compared to $SOS_{current}$, with an average delay of about 1.24 days (Fig. 1a). Conversely, for the non-drought years, only 43.0% of vegetated areas show delayed SOS_{next}, with a slight advancement of -0.14 days (Fig. 1b). This advancement aligns with previous reports of spring advancements (0.1–0.8 days) due to global warming[8,15,29,30].

We also used phenology models to account for the predominant environmental determinants influencing spring phenology, thus better

https://doi.org/10.1038/s41558-025-02273-6

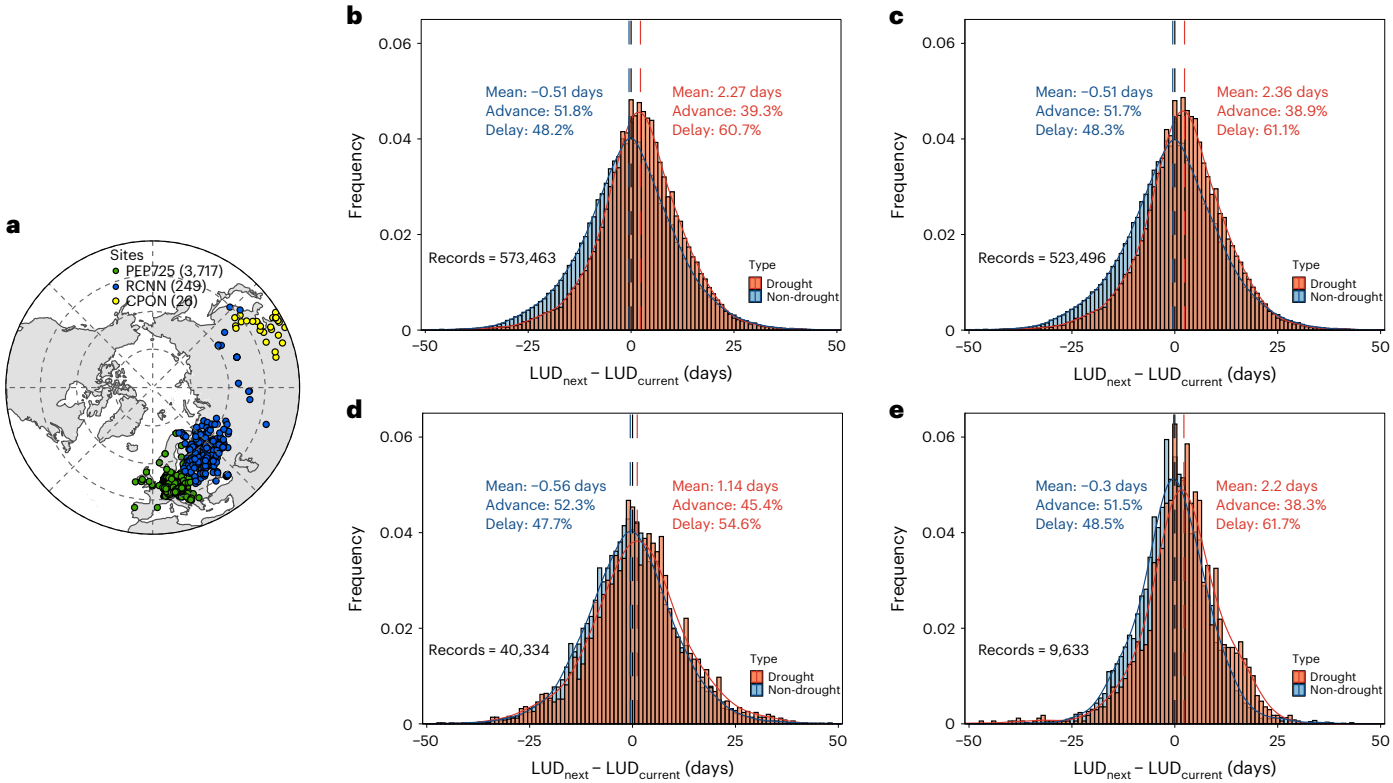

Fig. 2 | Effects of drought on LUD of next year using ground-based observations from three phenological networks. a, Locations of the ground-based phenological observations. **b**–**e**, Changes in $LUD_{next} - LUD_{current}$ when drought occurred or not using all ground-based phenological observations (**b**), PEP725 observations (1945–2016) (**c**), RCNN observations (1901–2017) (**d**) and CPON observations (1963–2014) (**e**).

isolating drought legacy effects (model-based method). To do so, we optimized five distinct phenology models considering the influence of temperature and photoperiod to predict SOS (SOS_{pred}), using phenology records unaffected by drought events (Methods). Subsequently, we calculated ΔSOS, by comparing the observed SOS after drought (SOS_{obs}) with SOS_{pred}. This allows us to isolate the impact of drought on SOS that is not accounted for by the models. As expected, SOS_{pred} closely approximates SOS_{obs} for non-drought years (Fig. 1d). In contrast, for years following droughts, 57.3% of the area exhibit delayed SOS compared to the model predictions, with an average delay of ~0.75 days (Fig. 1c). This model-based method shows a smaller difference in ΔSOS between drought and non-drought years (0.75 days) compared to the observation-based method (1.24 days), probably due to covariation of winter and spring temperatures with droughts, partly explaining delayed SOS_{next}. Nonetheless, these findings collectively indicate that drought legacy effects can substantially delay SOS, with an effect nearly one order of magnitude stronger than advances induced by warming. Even when we consider the frequency of the drought events, the equivalent annual delay of SOS_{next} induced by drought legacy is still twice as large as warming, particularly in mid-latitude regions (Extended Data Fig. 2).

To validate satellite-based analyses, we calculated differences in leaf unfolding dates ($\Delta LUD = LUD_{next} - LUD_{current}$) using 573,463 ground-based phenological records from 1901 to 2017 across three phenological networks in Europe, China and Russia (PEP725, CPON and RCNN) spanning different Northern Hemisphere climate zones (Fig. 2a). We observed an 2.27 days delay in LUD_{next} during drought compared to a slight advance of −0.51 days during non-drought years (Fig. 2b). Specifically, among the three ground phenological networks, droughts delay LUD_{next} by 2.36 and 2.20 days for PEP725 and CPON, respectively, but only 1.14 days for RCNN (Fig. 2c,e,d). PEP725 and CPON also exhibit a higher proportion of delayed SOS (61.1% and 61.7%, respectively) compared to RCNN (54.6%). These results are consistent across eight major species, with delays averaging from 1.69 to 4.87 days (Extended Data Fig. 3).

To better understand the legacy effects of drought on spring phenology, we categorized drought events into three types based on the recovery time of SM (Methods; Extended Data Fig. 1 and Fig. 3a–c). SM for type 1 droughts did not recover until the start of the next spring, thus affecting spring phenology through both endogenous and exogenous memory effects. Type 2 and type 3 droughts exhibit mostly endogenous memory effects, but differ in whether SM recovered within the growing season, which influences the strength of memory effect, due to differences in drought severity and duration (Supplementary Figs. 2 and 3).

We used the observation-based ($SOS_{next} - SOS_{current}$) and model-based ($SOS_{obs} - SOS_{pred}$) methods to assess the legacy effects of these three drought types on spring phenology. Both approaches consistently show that SOS exhibits a stronger delay for type 1 and type 2 droughts compared to type 3, with a larger proportion of delayed pixels and a greater average delay (Fig. 3). This is expected given that type 3 droughts are generally less severe than the other types. Moreover, the impact of type 1 drought displays a latitudinal pattern, with noticeable delays observed in mid-latitude regions and slight delays or even advancement in high latitudes (Fig. 3d,g). Interestingly, type 1 droughts show a larger discrepancy between observation-based and model-based methods compared to the other types (Fig. 3d,g). This may be attributed to the exogenous memory effect of drought via temperature, partially accounted for by phenology models.

Controlling factors and underlying mechanisms

To explore the underlying mechanisms of drought legacies on SOS, we constructed random forest (RF) models using climate variables, plant characteristics, soil properties and drought-related variables to predict the SOS anomalies of the next year ($SOS_{next} - SOS_{current}$) for

https://doi.org/10.1038/s41558-025-02273-6

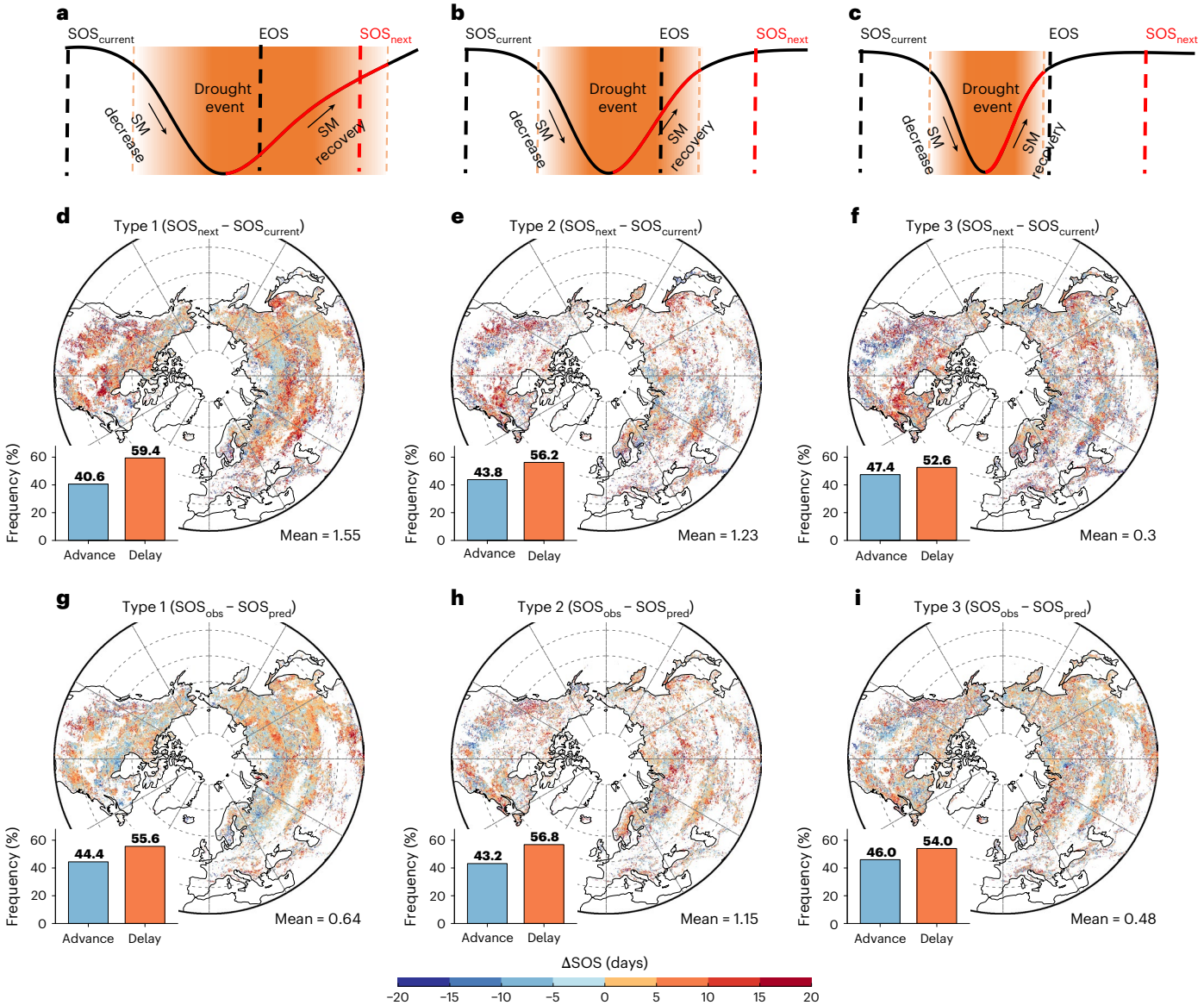

Fig. 3 | Effects of three types of drought on the SOS of the next year. **a**–**c**, Schematic diagrams of three drought types, SM did not recover until the start of the next growing season (type 1) (**a**), SM recovered before the next growing season (type 2) (**b**) and SM recovered within the current growing season (type 3) (**c**). **d**–**i**, The spatial patterns of the drought effect on the SOS of the next year for type 1 (**d**,**g**), type 2 (**e**,**h**) and type 3 (**f**,**i**), calculated through the observation-based method (**d**,**e**,**f**) and the model-based method (**g**,**h**,**i**). Insets show the area fraction of SOS delayed (orange) or advanced (blue) by drought.

each of the three drought types. These variables can be categorized into dynamic variables related to each drought event and static variables related to the background environmental conditions (Methods; Supplementary Table 2). On average, the resulting models explain 59.5% of variability in ΔSOS (61.4% for type 1, 56.2% for type 2 and 55.4% for type 3, respectively). On the basis of these models, we derived the relative importance ranking of each variable and partial dependence contribution to the SOS anomalies of the next year (Fig. 4).

Across all drought types, climate variables exert the greatest influence on the SOS changes after drought of the next year, followed by drought characteristics, plant characteristics and soil properties. Postdrought winter and spring temperatures exhibit the strongest influence, aligning with the known importance of winter chilling requirement and spring heat accumulation necessary to initiate biological spring, a mechanism embedded in most phenology models[31]. Background climate conditions are also critical, as drought causes greater SOS delays in dry regions. The effect of mean annual temperature varies across drought types: warmer regions experience greater delays for type 1 drought, whereas colder regions show stronger delays for types 2 and 3 droughts. In warmer regions, preseason water availability plays a crucial role in initiating leaf unfolding compared to temperature[32]. This also explains the less optimal performance of temperature and photoperiod models in water-limited areas (Supplementary Fig. 4).

Among variables related to individual drought event, spring SM anomalies notably affect SOS changes, with negative anomalies delaying SOS for type 1 but advancing SOS for type 2 and type 3 droughts. Ecosystems experiencing longer drought durations and greater SM losses tend to delay SOS, particularly evident for type 1 droughts. For type 2 and type 3 droughts, as spring SM have recovered from drought, additional SM may reduce oxygen and nutrient availability, delaying leaf-out.

Regarding plant responses to each drought event, negative anomalies in gross primary productivity (GPP) were associated with larger delays in SOS across all three drought types. Earlier end of season (EOS) also leads to slight SOS delays, particularly for type 1 drought occurring

https://doi.org/10.1038/s41558-025-02273-6

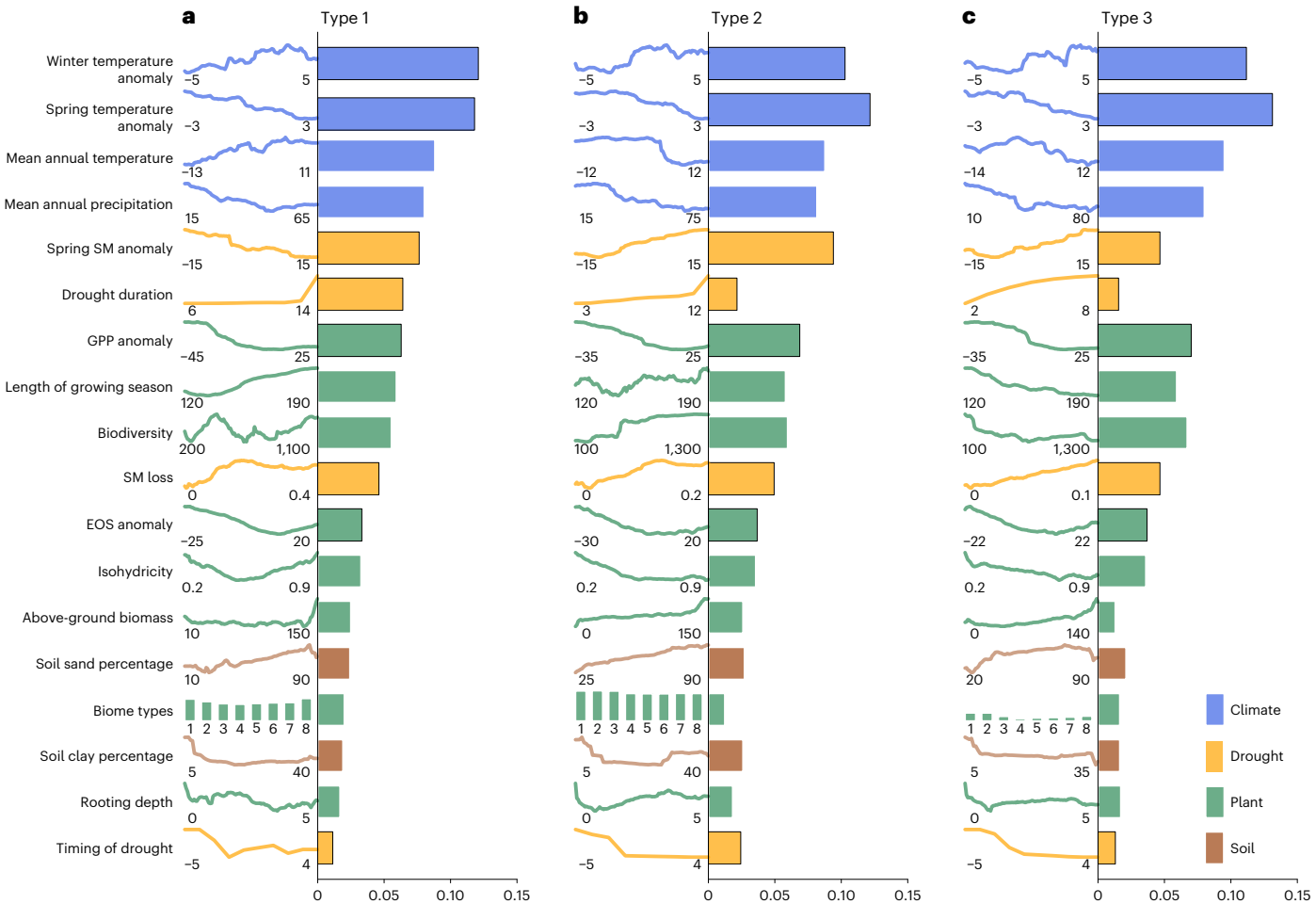

Fig. 4 | Response functions for SOS changes (SOS_{next} − $SOS_{current}$) following three types of drought. a–**c**, Results from three RF models for type 1 (**a**), type 2 (**b**) and type 3 (**c**) droughts. Left side of each panel displays the response functions, with numbers in the bottom left and right indicating the lower and upper bounds of independent variables, respectively. Bars on the right side represent variable importance. Variables with black borders are time-varying for each specific drought event, while others are static variables. Code for biome types: 1, temperate broadleaf and mixed forests; 2, temperate coniferous forests; 3, boreal forests/taiga; 4, temperate grasslands, savannas and shrublands; 5, montane grasslands and shrublands; 6, tundra; 7, Mediterranean forests; and 8, xeric shrublands.

between 45° and 55° N (Extended Data Fig. 4f). We also observe considerable impact of ecosystem characteristics on the SOS changes of the next year. Ecosystems with longer growing seasons, higher biodiversity and lower isohydricity values (more isohydric behaviour) tend to delay SOS after droughts. Although higher biodiversity can enhance ecosystem resistance to mild droughts (type 3), but severe droughts (types 1 and 2) require longer recovery times[33,34]. Droughts tend to delay SOS more for plants with stricter water status regulation (isohydric plants), probably due to greater reduction in carbon assimilation during drought[35,36]. Other factors, particularly those related to soil characteristics, exert a relatively weaker influence on SOS.

We also trained RF models to predict the SOS changes of the next year estimated by the model-based method (SOS_{obs} − SOS_{pred}). Even after eliminating the influence of temperature and photoperiod through phenology models, the resulting RF models can still explain 50.2% of the SOS changes of the next year (52.2% for type 1, 46.0% for type 2 and 43.3% for type 3, respectively), which also show similar environmental dependencies (Extended Data Fig. 5).

Exogenous and endogenous memory effect of drought

We used path analysis to differentiate the endogenous and exogenous memory effects of droughts on SOS. Droughts exhibit stronger legacy effects in drylands compared to wet regions (Fig. 5), which peaks in semi-arid areas (Extended Data Fig. 6b). Notably, the influence of exogenous effects dominates the legacy effect (Fig. 5 and Extended Data Figs. 6 and 7), primarily through diminishing spring SM (Ex1). Although drought legacies can also delay SOS through reduced spring temperatures (Ex2), this pathway generally exhibits weaker effects compared to SM in most biomes, with exceptions observed in temperate coniferous forests and temperate grasslands (Extended Data Fig. 7b,f). This exogenous effect via spring temperatures (Ex2) may also explain the greater disparities between observation-based and model-based methods for type 1 droughts (Fig. 3a,d). The legacy effect diminishes in high-latitude areas (for example, boreal forests/taiga regions) and even reverses in tundra regions (Extended Data Fig. 7c,d), probably due to strong cold stress and relatively weaker water limitations. This finding aligns with our analysis indicating that RCNN shows less delay in SOS compared to PEP725 and CPON (Fig. 2d,c,e). Additionally, endogenous memory effects also delay SOS, especially through reduced GPP during the drought period (En1). These endogenous effects are generally one-fifth to half as strong as the exogenous effects but are relatively more pronounced in temperate broadleaf/mixed forests, temperate coniferous forests and Mediterranean forests (Extended Data Fig. 7a,b,g).

Our research underscores the importance of exogenous memory effects in delaying SOS following droughts. Drought-induced SM

https://doi.org/10.1038/s41558-025-02273-6

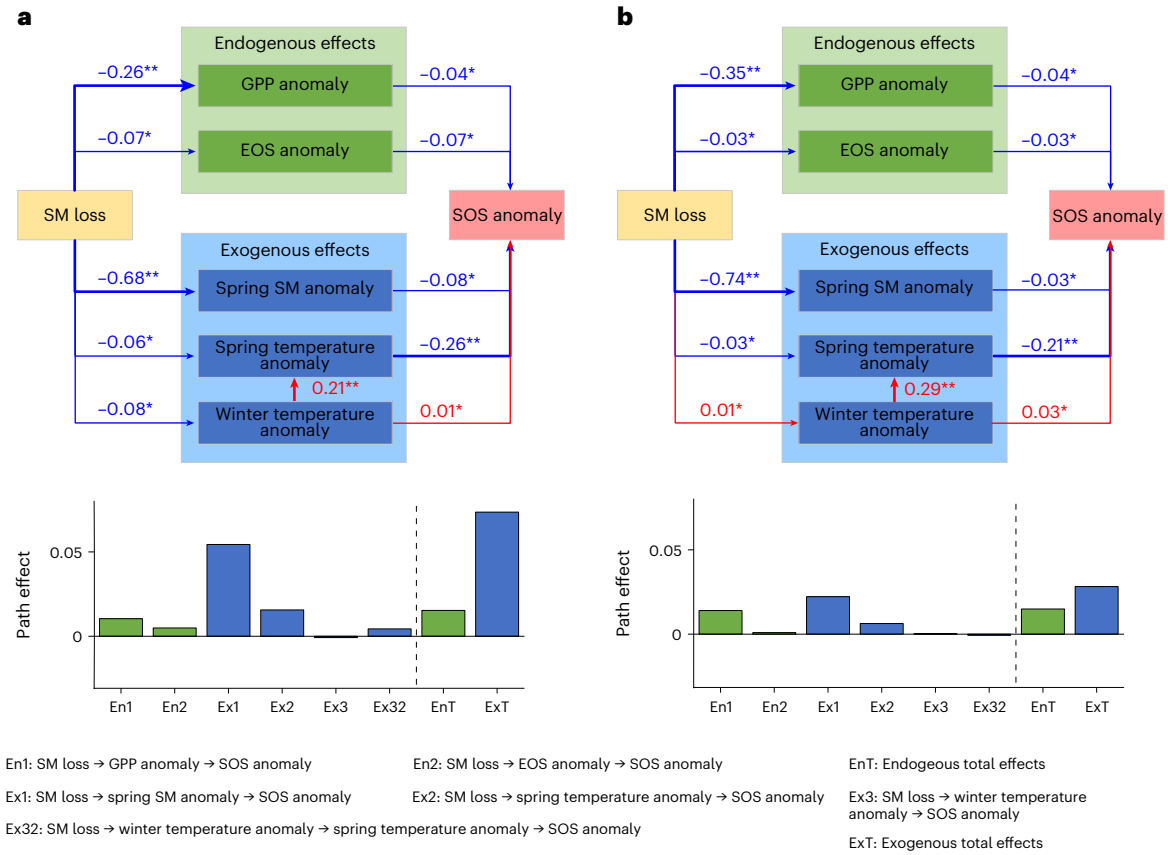

Fig. 5 | Path diagrams illustrating the underlying mechanisms of legacy effect of drought. a,**b**, Results from path diagrams for drylands (**a**) and wet regions (**b**). The numbers represent the mean of standardized path coefficients; asterisks denote the significance levels (**$P < 0.01$; *$P < 0.05$). The colours and widths of the arrows represent the signs (blue for negative, red for positive) and magnitudes of the path coefficients, respectively. The significance was based on a two-tailed Student's *t*-test. En1, En2, Ex1, Ex2, Ex3 and Ex32 indicate the effect of six major paths; EnT is the total endogenous effect; and ExT is the total exogenous effect.

deficits may carry over to the next spring and hinder leaf expansion, especially in arid and semi-arid regions (Fig. 5 and Extended Data Fig. 6). In these regions (montane grasslands and temperate grasslands), plants are strongly constrained by water availability[37,38], making them more susceptible to the exogenous memory effects of drought. As trees become dominant with decreasing aridity[39], the relative importance of exogenous memory effects declines (Extended Data Figs. 6 and 7). Soil water deficits are also more likely to recover within a growing season in these wet regions (Supplementary Figs. 2 and 3), resulting in a weaker exogenous memory effect. Under extreme conditions, such as in high-latitude tundra ecosystems, drought-induced spring SM decline may advance SOS, possibly due to decreased snow cover, reduced inundation and accelerated soil thawing[40,41]. Additionally, drought legacies may delay SOS through reductions in spring or winter temperature (Ex2, Ex3 and Ex32 in Fig. 5). However, these pathways are generally weaker and may involve large-scale circulation changes and complex land–atmosphere feedbacks, thus exhibiting a geographical dependence (Extended Data Fig. 7).

The endogenous effect also delays SOS in the Northern Hemisphere, albeit with a relatively weaker effect size than exogenous factors. Although we primarily used GPP anomalies as the major indicator of endogenous regulation, it may also reflect processes related to reductions in non-structural carbon storage[42,43] and enhanced xylem embolism[44,45], which are processes hypothesized to play a key role in causing drought legacy effects. Accordingly, we found that forest ecosystems exhibited stronger endogenous effects than grasslands (Extended Data Fig. 7). Evidence from phloem girdling experiments also suggest that availability of internal carbon reserves is a decisive factor in determining whether trees can initiate the energetically costly process of leaf growth[46]. Reduced carbon storage often delays spring leaf-out in temperate trees[46], whereas warming-induced increases in carbon uptake are associated with earlier spring phenology in temperate and boreal regions. Such mechanism can also explain the legacy effect from the carbon sink limitation perspective[20]. Reductions in GPP during drought years can be as large as −12.0 gC m^{-2} yr^{-1} for type 1 drought (Extended Data Fig. 8a), which can be further exacerbated by additional carbon costs for future xylem regrowth, both contributing to the negative correlation between GPP anomalies and SOS anomalies (Figs. 4 and 5). Endogenous memory via the EOS pathway also contributes to the SOS of the following year (Extended Data Fig. 5), probably because nutrient resorption is inhibited due to earlier leaf abscission[47]. Our analysis also revealed that the deficiency in soil nutrient (Extended Data Fig. 9), particularly soil nitrogen content, exacerbates the endogenous memory effects of drought, leading to delayed spring phenology for the subsequent year. Adequate soil nitrogen availability plays a pivotal role in speeding up the rejuvenation of plant growth and metabolic processes during drought recovery[48]. This finding is consistent with a previous study indicating a stronger nitrogen limitation in the Northern Hemisphere compared to phosphorus[49].

However, it should be noted that many endogenous factors—such as life traits which directly affect the recovery of xylem embolism and hormones levels—are not accurately considered at this ecosystem-level analysis. These characteristics may in part explain the differences in legacy effect at species level. For example, our analysis based on in situ observations indicates that *Tilia cordata* Mill. and *Tilia. platyphyllos* Scop. exhibit the most pronounced delay in LUD_{next} following drought events (Extended Data Fig. 3g,h). This can be attributed to stronger drought legacy effects in diffuse-porous species[50]. Although these

species are generally more drought-resistant[51], they rely heavily on the xylem produced in previous years for the water transport[52], thereby delaying the recovery of hydraulic conductivity after embolism[50]. Conversely, ring-porous species can restore their hydraulic conductivity by developing fresh xylem before budbreak[53], which typically results in weaker legacy effects. This mechanism probably explains the smaller delay in LUD_{next} for *Aesculus hippocastanum* L. and *Quercus robur* L. (Extended Data Fig. 3a,e). However, such recovery often requires additional non-structural carbon cost, whose effects may diminish when repeated drought happens. Consistent with previous studies[50], the non-porous species *Larix decidua* Mill. shows the weakest legacy effect (Extended Data Fig. 3d). Additionally, several phytohormones, such as cytokinin and abscisic acid, also regulate the enzyme activity and leaf rejuvenation and growth[54,55], thereby regulating leaf unfolding and plant resilience to drought. However, these factors are not considered in this study because of the lack of observations. Thus, the reported weak endogenous effect is likely to be underestimated and warrant further investigation.

Global warming has led to a continuous advancement of spring green-up[56]. While we are enhancing our understanding of how the SOS affects drought responses[57], much less is known about how drought in turn affects subsequent spring phenology. Using the long-term remote sensing observations and ground-based phenological records, we found that the legacy effects of droughts considerably delay the green-up and leaf unfolding of the next spring, with an effect size almost one order of magnitude stronger than the annual warming-induced advances. However, the effect of drought on SOS trend also strongly depends on the changes of drought severity and frequency. With projected increases of drought frequency and intensity induced by global warming and vegetation greening[3,23], such drought legacies are expected to constrain the response of SOS to global warming. Together with photoperiod constraints[58] and decreases in chilling requirements[18], the advancement of SOS may diminish and even reverse in the future. Given the importance of spring phenology in regulating spring carbon uptake[5] and its legacy impacts on autumn leaf senescence[10,12], incorporating the effects of drought legacies in phenology models and the interactions between drought legacies and spring phenology into Earth system models is crucial for improving predictions of ecosystem responses to extreme climate events. Future studies based on manipulative experiments may offer more mechanistic understanding, thereby necessitating model improvements.

Online content

Any methods, additional references, Nature Portfolio reporting summaries, source data, extended data, supplementary information, acknowledgements, peer review information; details of author contributions and competing interests; and statements of data and code availability are available at https://doi.org/10.1038/s41558-025-02273-6.

References

1. Barichivich, J. et al. Large-scale variations in the vegetation growing season and annual cycle of atmospheric CO_2 at high northern latitudes from 1950 to 2011. *Glob. Change Biol.* **19**, 3167–3183 (2013).
2. Menzel, A. et al. European phenological response to climate change matches the warming pattern. *Glob. Change Biol.* **12**, 1969–1976 (2006).
3. Myneni, R. B., Keeling, C. D., Tucker, C. J., Asrar, G. & Nemani, R. R. Increased plant growth in the northern high latitudes from 1981 to 1991. *Nature* **386**, 698–702 (1997).
4. Peñuelas, J. & Filella, I. Phenology. Responses to a warming world. *Science* **294**, 793–795 (2001).
5. Keenan, T. F. et al. Net carbon uptake has increased through warming-induced changes in temperate forest phenology. *Nat. Clim. Change* **4**, 598–604 (2014).
6. Dragoni, D. et al. Evidence of increased net ecosystem productivity associated with a longer vegetated season in a deciduous forest in south-central Indiana, USA. *Glob. Change Biol.* **17**, 886–897 (2011).
7. Lian, X. et al. Seasonal biological carryover dominates northern vegetation growth. *Nat. Commun.* **12**, 983 (2021).
8. Xu, X., Riley, W. J., Koven, C. D., Jia, G. & Zhang, X. Earlier leaf-out warms air in the north. *Nat. Clim. Change* **10**, 370–375 (2020).
9. Kharouba, H. et al. Global shifts in the phenological synchrony of species interactions over recent decades. *Proc. Natl Acad. Sci. USA* **115**, 201714511 (2018).
10. Zani, D., Crowther, T. W., Mo, L., Renner, S. S. & Zohner, C. M. Increased growing-season productivity drives earlier autumn leaf senescence in temperate trees. *Science* **370**, 1066–1071 (2020).
11. Wang, H.-L. et al. An alternative splicing variant of PtRD26 delays leaf senescence by regulating multiple NAC transcription factors in *Populus*. *Plant Cell* **33**, 1594–1614 (2021).
12. Keenan, T. F. & Richardson, A. D. The timing of autumn senescence is affected by the timing of spring phenology: implications for predictive models. *Glob. Change Biol.* **21**, 2634–2641 (2015).
13. Buermann, W. et al. Widespread seasonal compensation effects of spring warming on northern plant productivity. *Nature* **562**, 110–114 (2018).
14. Zhang, Y., Keenan, T. F. & Zhou, S. Exacerbated drought impacts on global ecosystems due to structural overshoot. *Nat. Ecol. Evol.* **5**, 1490–1498 (2021).
15. Piao, S. et al. Plant phenology and global climate change: current progresses and challenges. *Glob. Change Biol.* **25**, 1922–1940 (2019).
16. Sills, J., Chuine, I., Morin, X. & Bugmann, H. Warming, photoperiods, and tree phenology. *Science* **329**, 277–278 (2010).
17. Fu, Y. H. et al. Daylength helps temperate deciduous trees to leaf-out at the optimal time. *Glob. Change Biol.* **25**, 2410–2418 (2019).
18. Fu, Y. H. et al. Declining global warming effects on the phenology of spring leaf unfolding. *Nature* **526**, 104–107 (2015).
19. Zhang, H., Chuine, I., Regnier, P., Ciais, P. & Yuan, W. Deciphering the multiple effects of climate warming on the temporal shift of leaf unfolding. *Nat. Clim. Change* **12**, 193–199 (2022).
20. Gu, H. et al. Warming-induced increase in carbon uptake is linked to earlier spring phenology in temperate and boreal forests. *Nat. Commun.* **13**, 3698 (2022).
21. Müller, L. M. & Bahn, M. Drought legacies and ecosystem responses to subsequent drought. *Glob. Change Biol.* **28**, 5086–5103 (2022).
22. Kannenberg, S. A. et al. Linking drought legacy effects across scales: from leaves to tree rings to ecosystems. *Glob. Change Biol.* **25**, 2978–2992 (2019).
23. Petrova, I. Y. et al. Observation-constrained projections reveal longer-than-expected dry spells. *Nature* **633**, 594–600 (2024).
24. Trenberth, K. E. et al. Global warming and changes in drought. *Nat. Clim. Change* **4**, 17–22 (2014).
25. Estiarte, M. & Peñuelas, J. Alteration of the phenology of leaf senescence and fall in winter deciduous species by climate change: effects on nutrient proficiency. *Glob. Change Biol.* **21**, 1005–1017 (2015).
26. Cleverly, J. et al. Soil moisture controls on phenology and productivity in a semi-arid critical zone. *Sci. Total Environ.* **568**, 1227–1237 (2016).
27. Ji, S. et al. Diverse responses of spring phenology to preseason drought and warming under different biomes in the North China Plain. *Sci. Total Environ.* **766**, 144437 (2020).
28. Zeng, Z. et al. Legacy effects of spring phenology on vegetation growth under preseason meteorological drought in the Northern Hemisphere. *Agric.Meteorol.* **310**, 108630 (2021).

29. Jeong, S.-J., HO, C.-H., GIM, H.-J. & BROWN, M. E. Phenology shifts at start vs. end of growing season in temperate vegetation over the Northern Hemisphere for the period 1982–2008. *Glob. Change Biol.* **17**, 2385–2399 (2011).
30. Fu, Y. H. et al. Recent spring phenology shifts in western Central Europe based on multiscale observations. *Glob. Ecol. Biogeogr.* **23**, 1255–1263 (2014).
31. Wang, H. et al. Overestimation of the effect of climatic warming on spring phenology due to misrepresentation of chilling. *Nat. Commun.* **11**, 4945 (2020).
32. Shen, M. et al. Plant phenology changes and drivers on the Qinghai–Tibetan Plateau. *Nat. Rev. Earth Environ.* **3**, 633–651 (2022).
33. Isbell, F. et al. Biodiversity increases the resistance of ecosystem productivity to climate extremes. *Nature* **526**, 574–577 (2015).
34. Liu, D., Wang, T., Peñuelas, J. & Piao, S. Drought resistance enhanced by tree species diversity in global forests. *Nat. Geosci.* **15**, 800–804 (2022).
35. Nolan, R. H. et al. Differences in osmotic adjustment, foliar abscisic acid dynamics, and stomatal regulation between an isohydric and anisohydric woody angiosperm during drought. *Plant Cell Environ.* **40**, 3122–3134 (2017).
36. Wu, C. et al. Increased drought effects on the phenology of autumn leaf senescence. *Nat. Clim. Change* **12**, 943–949 (2022).
37. Jiao, W. et al. Observed increasing water constraint on vegetation growth over the last three decades. *Nat. Commun.* **12**, 3777 (2021).
38. Zhang, W. et al. Divergent response of vegetation growth to soil water availability in dry and wet periods over Central Asia. *J. Geophys. Res. Biogeosci.* **126**, e2020JG005912 (2021).
39. Poppenwimer, T., Mayrose, I. & DeMalach, N. Revising the global biogeography of annual and perennial plants. *Nature* **624**, 109–114 (2023).
40. Wang, X. et al. Disentangling the mechanisms behind winter snow impact on vegetation activity in northern ecosystems. *Glob. Change Biol.* **24**, 1651–1662 (2018).
41. Li, T. et al. Soil freeze–thaw cycles affect spring phenology by changing phenological sensitivity in the Northern Hemisphere. *Sci. Total Environ.* **914**, 169963 (2024).
42. Bazot, S., Fresneau, C., Damesin, C. & Barthes, L. Contribution of previous year's leaf N and soil N uptake to current year's leaf growth in sessile oak. *Biogeosciences* **13**, 3475–3484 (2016).
43. Han, Q. & Kabeya, D. Recent developments in understanding mast seeding in relation to dynamics of carbon and nitrogen resources in temperate trees. *Ecol. Res.* **32**, 771–778 (2017).
44. Adams, H. D. et al. A multi-species synthesis of physiological mechanisms in drought-induced tree mortality. *Nat. Ecol. Evol.* **1**, 1285–1291 (2017).
45. Zeppel, M. J. B. et al. Embolism recovery strategies and nocturnal water loss across species influenced by biogeographic origin. *Ecol. Evol.* **9**, 5348–5361 (2019).
46. Amico, R. A., Jessica, O., Paula, G.-D. & Zwieniecki, M. A. Spring phenology is affected by fall non-structural carbohydrates concentration and winter sugar redistribution in three Mediterranean nut tree species. *Tree Physiol.* **41**, 1425–1438 (2021).
47. Vergutz, L., Manzoni, S., Porporato, A., Novais, R. F. & Jackson, R. B. Global resorption efficiencies and concentrations of carbon and nutrients in leaves of terrestrial plants. *Ecol. Monogr.* **82**, 205–220 (2012).
48. Mason, R. E. et al. Evidence, causes, and consequences of declining nitrogen availability in terrestrial ecosystems. *Science* **376**, eabh3767 (2022).
49. Du, E. et al. Global patterns of terrestrial nitrogen and phosphorus limitation. *Nat. Geosci.* **13**, 221–226 (2020).
50. Kannenberg, S. A. et al. Drought legacies are dependent on water table depth, wood anatomy and drought timing across the eastern US. *Ecol. Lett.* **22**, 119–127 (2019).
51. Tyree, M. & Ewers, F. The hydraulic architecture of trees and other woody plants. *New Phytol.* **119**, 345–360 (1991).
52. Zimmermann, M. H. *Xylem Structure and the Ascent of Sap* (Springer, 1983).
53. Pérez-de-Lis, G., Rossi, S., Vázquez-Ruiz, R. A., Rozas, V. & García-González, I. Do changes in spring phenology affect earlywood vessels? Perspective from the xylogenesis monitoring of two sympatric ring-porous oaks. *New Phytol.* **209**, 521–530 (2016).
54. Mughal, N. et al. Adaptive roles of cytokinins in enhancing plant resilience and yield against environmental stressors. *Chemosphere* **364**, 143189 (2024).
55. Singh, A. & Roychoudhury, A. Abscisic acid in plants under abiotic stress: crosstalk with major phytohormones. *Plant Cell Rep.* **42**, 961–974 (2023).
56. Piao, S. et al. Leaf onset in the northern hemisphere triggered by daytime temperature. *Nat. Commun.* **6**, 6911 (2015).
57. Li, Y. et al. Widespread spring phenology effects on drought recovery of Northern Hemisphere ecosystems. *Nat. Clim. Change* **13**, 182–188 (2023).
58. Way, D. A. & Montgomery, R. A. Photoperiod constraints on tree phenology, performance and migration in a warming world. *Plant Cell Environ.* **38**, 1725–1736 (2015).

Methods

Satellite-derived SOS observations

Third generation of GIMMS (3g) from the advanced very high-resolution radiometer (AVHRR)[59] was applied to extract vegetation phenology in northern ecosystems (>30° N) during 1982–2015. We first excluded non-vegetated and sparse vegetation coverage (annual mean NDVI < 0.1) and cropland on the basis of the MODIS land cover climate modelling grid (MCD12C1)[60]. Second, NDVI was contaminated by snow cover in high latitudes during spring and winter, seriously affecting the accuracy of phenological extraction. For lack of snow information, we used daily temperature data to identify potential snow cover, and snow-cover periods were identified as the period when the air temperature was <0 °C for at least five consecutive days. The snow-contaminated NDVIs were replaced by the mean of 75 to 95 percentiles of snow-free NDVIs in winter. Third, Savitzky–Golay filter was applied to reconstructed NDVI time series to further minimize noise from atmospheric contamination[61]. Fourth, we interpolated daily NDVI using six-order polynomial time-series model, and then phenology was determined by the dynamic-threshold method[62]. The date when NDVI first surpasses 20% of its annual amplitude was defined as SOS[63], and the EOS was identified as the date when NDVI decreased by 50% of its annual amplitude[64] (Supplementary Fig. 1).

Ground SOS observations

The ground-based SOS was obtained from three phenological observation networks, including PEP725 (ref. 65), CPON[66] and RCNN[67]. Owing to different definitions of SOS for these three ground phenological network, we screened the phenological observations according to the following criteria. In PEP725 network, SOS was represented by the date of first visible leaf stalk (phenological phase code (BBCH) = 11)[65], and ultimately 232,633 LUD records were available for eight species at 1,321 sites, with at least 30 years of consecutive records during 1951–2015. For CPON, we used leaf-out date to represent SOS[68] and 19,622 SOS records of 513 species at 44 sites with at least 5 years of observations between 1963 and 2015. In RCNN, SOS was the leaf-out stage[67] and we only retained SOS records with Quality = OK, resulting in 15,800 SOS records of 189 species at 117 sites for at least 5 years of observations during 1927–2015. In total, 280,369 SOS records of 870 species at 1,913 sites were used in this study.

Drought identification

Since SM better indicates the water stress on plants compared to meteorological drought indices[69], during the satellite era (1982 to 2015) when SM data are available, we used monthly root-zone SM from GLEAM v.3.7a (ref. 70) together with monthly NDVI to identify drought events. First, we deseasonalized and detrended SM and NDVI by subtracting the multi-year monthly average and linear trend to eliminate seasonal influences as well as the long-term trend. Then, we calculated the standard deviation of the detrended SM and NDVI, and defined their negative anomaly as <−0.5 s.d. We focus on 'effective drought events', which refer to droughts that have negative impacts on ecosystems[71]. Specifically, we defined the drought event as a period when SM anomaly lasted at least for two consecutive months during the growing season, and NDVI anomaly also occurred during this period for at least one month. According to the recovery time of SM (SM anomaly returning above 0), drought events can be divided into three types: SM has not recovered before the next spring (type 1), recovers before the next spring (type 2) and SM recovers during the current growing season (type 3) (Extended Data Fig. 1). The statistics of three types of drought events are shown in Supplementary Figs. 2 and 3.

For long-term ground observation, standardized precipitation evapotranspiration index (SPEI) data were used for identifying drought events (SPEIbase v.2.7)[72], because of the lack of reliable SM records that cover the necessary length of time for this analysis. SPEI is a widely used indicator to characterize meteorological drought by calculating the standardized water balance anomalies at different timescales[72]. To capture the short-term water deficit, 3-month SPEI (SPEI3) was used in this study and we defined drought events as two consecutive months of SPEI3 <−1.5 during the growing season (March to October), since it exhibits a similar spatial distribution to the above method using both SM and NDVI (Supplementary Fig. 5 versus Supplementary Fig. 2).

The influence of drought events on spring phenology

We used two methods to evaluate the legacy effect of current year drought events on the spring phenology of the next year.

Method 1 (observation-based method). The main basis is that plants normally exhibit slightly changes in SOS between adjacent years. We first calculated the difference in SOS between all consecutive years (equation (1)) and then identified whether a drought event occurred or not during those years. Since $SOS_{current}$ was set as a baseline unaffected by drought, we removed the sample if drought occurred before $SOS_{current}$. For instance, there was no drought in 1982, whereas a drought occurred in 1983 and the impact of drought on SOS is defined as the difference between SOS_{1984} and SOS_{1983}. If there were no droughts in 1982 and 1983, $SOS_{1984} - SOS_{1983}$ represents the difference in SOS under non-drought conditions.

$$\Delta SOS = SOS_{next} - SOS_{current} \quad (1)$$

Method 2 (model-based method). Parameter ΔSOS derived from the observation-based method may be obscured by the temperature anomalies. To eliminate the interference of temperature and photoperiod on the impact of drought on SOS, we calculated the difference between the observed and predicted SOS which is affected by drought (equation (2)). The SOS observations unaffected by drought events were used to parametrize the spring phenology model and predict the theoretical SOS for all years. Five phenological models were applied to predict SOS, including eco-dormancy release only model (thermal time model[73] and photothermal time model[74]) and endo- and eco-dormancy releases model (sequential model[75], parallel model[76] and unichill model[77]). Simulated annealing method were used to determine the optimization parameters of these models[78] using MATLAB R2022a. Since these models do not include any water stress metrics as predictors of SOS, any potential drought legacy effects will change the size of ΔSOS. The accuracy of the models was validated using root mean square error and significance level ($P < 0.05$) (Supplementary Fig. 4).

$$\Delta SOS = SOS_{obs} - SOS_{pred} \quad (2)$$

The thermal time model only considers the forcing process and calculates the cumulative temperature above T_{base} after 1 January (t_0) (equation (3)). SOS is defined as the date when forcing (S_f) is greater than its critical value (F_{crit}).

$$S_f = \sum_{t_0}^{t} \begin{cases} 0, & T \le T_{base} \\ T - T_{base}, & T > T_{base} \end{cases} \quad (3)$$

The photothermal time model considers the influence of both forcing and photoperiod, and the forcing is regulated by daylength (equation (4)).

$$S_f = \sum_{t_0}^{t} \begin{cases} 0, & T \le T_{base} \\ \frac{L_t}{24}(T - T_{base}), & T > T_{base} \end{cases} \quad (4)$$

The sequential model and parallel model use a triangular function (characterized by minimum (T_{min}), maximum (T_{max}) and optimum (T_{opt}) temperature) to accumulate chilling state (S_c) (equation (5)). Parameter S_c begins to accumulate after 1 September (t_c) of the previous year. The sequential model assumes that the accumulation of forcing will begin

when a chilling threshold (C_{crit}) is met ($K_{sequential}$, equation (6)). However, the parallel model assumes that chilling and forcing can increase simultaneously ($K_{parallel}$, equation (7)). The forcing begins to accumulate when T is greater than T_{base} and is controlled by the status of C_{crit} (equation (8)).

$$S_c = \sum_{t_c}^{t} \begin{cases} 0, & T \le T_{min}, \\ \frac{T - T_{min}}{T_{opt} - T_{min}}, & T_{min} < T \le T_{opt} \\ \frac{T - T_{max}}{T_{opt} - T_{max}}, & T_{opt} < T < T_{max} \\ 0, & T \ge T_{max} \end{cases} \quad (5)$$

$$K_{sequential} = \begin{cases} 0, & S_c < C_{crit} \\ 1, & S_c \ge C_{crit} \end{cases} \quad (6)$$

$$K_{parallel} = \begin{cases} K_{min} + \frac{1 - K_{min}}{C_{crit}} S_c, & S_c < C_{crit} \\ 1, & S_c \ge C_{crit} \end{cases} \quad (7)$$

$$S_f = \sum_{t_c}^{t} \begin{cases} K \frac{A_f}{1 + e^{\mathrm{alpha}(T + \mathrm{beta})}}, & T > T_{base} \\ 0, & T \le T_{base} \end{cases} \quad (8)$$

The unichill model accumulate chilling state using equation (9) and, similar to the sequential model, forcing cannot begin until C_{crit} is exceeded ($K_{unichill}$, equation (10)). The forcing process is calculated by a logistic function (equation (11)).

$$S_c = \sum_{t_c}^{t} \frac{1}{1 + e^{T_{min}(T - T_{max})^2 + T_{opt}(T - T_{max})}} \quad (9)$$

$$K_{unichill} = \begin{cases} 0, & S_c < C_{crit} \\ 1, & S_c \ge C_{crit} \end{cases} \quad (10)$$

$$S_f = \sum_{t_c}^{t} K \frac{1}{1 + e^{\mathrm{alpha}(T - \mathrm{beta})}} \quad (11)$$

Ultimately, we used the average results from the photothermal time model and the sequential models as SOS_{pred}, as they provide better model performance (Supplementary Fig. 4).

Factors affecting drought-induced SOS change

We used RF algorithms trained on 18 variables to explain the drought-induced SOS change, including spatial variables and drought-specific variables. The static variables include climate variables, for example, mean annual temperature (°C) and mean annual precipitation (mm) from CRU_TS v.4.05 (ref. 79); biotic variables, including mean length of growing season (LGS = EOS − SOS, days), maximum rooting depth (rooting depth, mm) from Plymouth Marine Laboratory[80], plant biodiversity from Anthroecology Lab[81], mean above-ground biomass (Mg ha^{-1}) from the Oak Ridge National Laboratory (ORNL) DAAC data repository[82], biomes types from Terrestrial Ecoregions of the World[83], and iso/anisohydry data (isohydricity) were produced on the basis of Ku-Band backscatter from QuikSCAT[84]; and soil texture (clay content and sand content, %)[85]. The dynamic variables include climate variables, for instance, spring temperature (March, April and May) anomaly after drought (ST anomaly, °C), winter temperature (December, January and February) anomaly after drought (WT anomaly, °C); biotic variables, including the absolute GPP anomaly in drought year (GPP anomaly, gC m^{-2})[86] and the EOS anomaly in drought year (EOS anomaly, days); and drought-related variables, for example, SM loss (the positive difference between −0.5 s.d. and detrended SM during drought, m^3 m^{-3}), the start month of the drought event (timing of drought, month), the length of time the drought event lasted (drought duration, months) and the spring SM anomaly after drought (SSM anomaly, m^3 m^{-3}). Detailed descriptions of all variables are given in Supplementary Table 2. It should be noted that we did not include spring and winter temperature anomalies as predictors in the model-based RF analysis, since their effects are already considered by the phenology models used to predict SOS_{pred}.

The RF is a widely used machine learning algorithm, which builds multiple regression trees using bootstrap resampling technique and recursive binary splitting[87]. We divided all data into two parts, with two-thirds used for a training model and the rest for validation. We finally built an RF model consisting of 500 regression trees with a leaf node size of 5. Using binary rules, regression tree recursively splits samples into two categories to minimize the variance in each category. The variable importance metric can be indicated by the number of splits; that is, the variable with larger number of splits is more important for predicting the response variable. Therefore, we used RF to evaluate the importance of variables on the change of the SOS after drought in the next year. In addition, partial dependent plot shows the response function of the predicted target variable (drought-induced SOS changes) to each covariate, providing the marginal effect of each covariate on the target variable. The analysis was conducted using the sklearn package in Python v.3.10.9.

Path analysis

Path analysis evaluates causal models by examining linear relationships between independent and dependent variables[88]. Unlike conventional multiple regression analysis, path analysis not only examines the direct influence of independent variables on dependent variables but also takes into account the interactions among independent variables and their indirect effects on dependent variables through intermediary variables. This approach enables a more precise estimation and examination of various hypothetical causal relationships by breaking down correlation coefficients into path coefficients. We used a path diagram to distinguish the endogenous and exogenous effects of drought on SOS. Endogenous legacy effects were defined as those caused by biological factors, whereby drought (indicated by SM loss) impacts vegetation physiology (GPP anomaly and EOS anomaly), and those physiological carryover effects that impact SOS. Exogenous legacy effects were considered as those arising from hydroclimatic legacies, whereby the hydroclimatic changes (spring SM anomaly, winter temperature anomaly and spring temperature anomaly) induced by the drought spilled over into the following year.

We used the lavaan package in R v.4.1.3 (ref. 89) to calculate the standardized path coefficients of the preset path diagram and calculated as the product of the standardized path coefficients along each pathway. We compared path effects of endogenous and exogenous by summing up the effects of individual response paths. In addition, dryland classification[90], biomes classification[83], soil nitrogen content (0–30 cm)[91] and soil phosphorous content (0–30 cm)[92] were used to examine the general characteristics of the path effects. Anomalies of variables (GPP, EOS, SSM, WT and ST) were calculated for each drought event in reference to its 34-yr (1982–2015) mean values. All variables were standardized before path analyses. We measured the adequacy of the fitness of the path diagram using the following criteria: goodness-of-fit index ≥ 0.95, comparative fit index ≥ 0.90, root mean square error of approximation ≤ 0.10 and standardized root mean square residual ≤ 0.05 (ref. 93).

Reporting summary

Further information on research design is available in the Nature Portfolio Reporting Summary linked to this article.

Data availability

The data that support the findings of this study are derived from the following resources. The PEP725 dataset can be downloaded from

www.pep725.eu. The RCNN dataset can be downloaded from https://doi.org/10.1038/s41597-020-0376-z. The CPON dataset can be downloaded from https://data.casearth.cn/dataset/5c19a5650600cf2a3c557ab1. The GIMMS NDVI 3g v.1 is available at https://data.tpdc.ac.cn/zh-hans/data/9775f2b4-7370-4e5e-a537-3482c9a83d88. The SM data are available at https://www.gleam.eu/. The SPEI dataset is available at https://spei.csic.es/database.html. The CRU climate dataset is available at https://crudata.uea.ac.uk/cru/data/hrg/. FLUXCOM GPP dataset can be downloaded from https://www.fluxcom.org/. The maximum root-depth data are available at https://wci.earth2observe.eu/thredds/catalog/usc/root-depth/catalog.html. The plant biodiversity data are available at http://ecotope.org/anthromes/biodiversity/plants/data/. The mean above-ground biomass data are available at https://daac.ornl.gov/cgi-bin/dsviewer.pl?ds_id=1763. The iso/anisohydry data are available via figshare at https://doi.org/10.6084/m9.figshare.5323987.v1 (ref. 94). The biomes data can be downloaded from https://www.worldwildlife.org/publications/terrestrial-ecoregions-of-the-world. The land cover data are available at https://lpdaac.usgs.gov/products/mcd12q1v006/. The soil properties data can be downloaded from https://daac.ornl.gov/SOILS/guides/HWSD.html. The soil total phosphorus concentration is available via figshare at https://doi.org/10.6084/m9.figshare.14583375 (ref. 95). The soil total nitrogen concentration is available at https://www.isric.org/explore/soilgrids/. Source data are provided with this paper.

Code availability

Main codes used for data processing in this study are available via figshare at https://doi.org/10.6084/m9.figshare.26130907 (ref. 96).

References

59. Pinzon, J. E. & Tucker, C. J. A non-stationary 1981–2012 AVHRR NDVI3g time series. *Remote Sens.* **6**, 6929–6960 (2014).
60. Friedl, M. & Sulla-Menashe, D. *MCD12C1 MODIS/Terra+Aqua Land Cover Type Yearly L3 Global 0.05Deg CMG V006* (NASA EOSDIS Land Processes Distributed Active Archive Center, 2015).
61. Chen, J. et al. A simple method for reconstructing a high-quality NDVI time-series data set based on the Savitzky–Golay filter. *Remote Sens. Environ.* **91**, 332–344 (2004).
62. White, M. A. et al. Intercomparison, interpretation, and assessment of spring phenology in North America estimated from remote sensing for 1982–2006. *Glob. Change Biol.* **15**, 2335–2359 (2009).
63. Shen, M. et al. Increasing altitudinal gradient of spring vegetation phenology during the last decade on the Qinghai–Tibetan Plateau. *Agric. For. Meteorol.* **189-190**, 71–80 (2014).
64. White, M. A., Thornton, P. E. & Running, S. W. A continental phenology model for monitoring vegetation responses to interannual climatic variability. *Glob. Biogeochem. Cycles* **11**, 217–234 (1997).
65. Templ, B. et al. Pan European phenological database (PEP725): a single point of access for European data. *Int. J. Biometeorol.* **62**, 1109–1113 (2018).
66. Zhu, M. et al. Mapping 24 woody plant species phenology and ground forest phenology over China from 1951 to 2020.*Earth Syst. Sci. Data* **16**, 277–293 (2024).
67. Ovaskainen, O. et al. Chronicles of nature calendar, a long-term and large-scale multitaxon database on phenology. *Sci. Data* **7**, 47 (2020).
68. Ge, Q., Wang, H., Rutishauser, T. & Dai, J. Phenological response to climate change in China: a meta-analysis. *Glob. Change Biol.* **21**, 265–274 (2015).
69. Chatterjee, S., Desai, A., Zhu, J., Townsend, P. & Huang, J. Soil moisture as an essential component for delineating and forecasting agricultural rather than meteorological drought. *Remote Sens. Environ.* **269**, 112833 (2022).
70. Martens, B. et al. GLEAM v3: satellite-based land evaporation and root-zone soil moisture. *Geosci. Model Dev.* **10**, 1903–1925 (2017).
71. Zhang, S., Yang, Y., Wu, X., Li, X. & Shi, F. Postdrought recovery time across global terrestrial ecosystems. *J. Geophys. Res. Biogeosci.* **126**, e2020JG005699 (2021).
72. Vicente-Serrano, S. M., Beguería, S., López-Moreno, J. I., Angulo, M. & El Kenawy, A. A new global 0.5° gridded dataset (1901–2006) of a multiscalar drought index: comparison with current drought index datasets based on the Palmer drought severity index. *J. Hydrometeorol.* **11**, 1033–1043 (2010).
73. Cannell, M. G. R. & Smith, R. I. L. Thermal time, chill days and prediction of budburst in *Picea sitchensis*. *J. Appl. Ecol.* **20**, 951–963 (1983).
74. Masle, J., Doussinault, G., Farquhar, G. D. & Sun, B. Foliar stage in wheat correlates better to photothermal time than to thermal time. *Plant Cell Environ.* **12**, 235–247 (1989).
75. Kramer, K. A modelling analysis of the effects of climatic warming on the probability of spring frost damage to tree species in The Netherlands and Germany. *Plant Cell Environ.* **17**, 367–377 (1994).
76. Landsberg, J. J. Apple fruit bud development and growth; analysis and an empirical model. *Ann. Bot.* **38**, 1013–1023 (1974).
77. Chuine, I. A unified model for budburst of trees. *J. Theor. Biol.* **207**, 337–347 (2001).
78. Kirkpatrick, S., Gelatt, C. D. & Vecchi, M. P. Optimization by simulated annealing. *Science* **220**, 671–680 (1983).
79. Harris, I., Osborn, T. J., Jones, P. & Lister, D. Version 4 of the CRU TS monthly high-resolution gridded multivariate climate dataset. *Sci. Data* **7**, 109 (2020).
80. Fan, Y., Miguez-Macho, G., Jobbágy, E., Jackson, R. & Otero Casal, C. Hydrologic regulation of plant rooting depth. *Proc. Natl Acad. Sci. USA* **114**, 201712381 (2017).
81. Ellis, E. C., Antill, E. C. & Kreft, H. All is not loss: plant biodiversity in the Anthropocene. *PLoS ONE* **7**, e30535 (2012).
82. Spawn, S. A. & Gibbs, H. K. *Global Aboveground and Belowground Biomass Carbon Density Maps for the Year 2010* (ORNL, 2020).
83. Olson, D. M. et al. Terrestrial ecoregions of the world: a new map of life on Earth. *Bioscience* **51**, 933–938 (2001).
84. Li, Y. et al. Estimating global ecosystem isohydry/anisohydry using active and passive microwave satellite data. *J. Geophys. Res. Biogeosci.* **122**, 3306–3321 (2017).
85. Wieder, W. *Regridded Harmonized World Soil Database v1.2* (ORNL, 2014).
86. Jung, M. et al. The FLUXCOM ensemble of global land–atmosphere energy fluxes. *Sci. Data* **6**, 74 (2019).
87. Fawagreh, K., Gaber, M. M. & Elyan, E. Random forests: from early developments to recent advancements. *Syst. Sci. Control Eng.* **2**, 602–609 (2014).
88. Streiner, D. L. Finding our way: an introduction to path analysis. *Can. J. Psychiatry* **50**, 115–122 (2005).
89. Rosseel, Y. lavaan: an R package for structural equation modeling. *J. Stat. Softw.* **48**, 1–36 (2012).
90. Zomer, R. J., Xu, J. & Trabucco, A. Version 3 of the global aridity index and potential evapotranspiration database. *Sci. Data* **9**, 409 (2022).
91. Poggio, L. et al. SoilGrids 2.0: producing soil information for the globe with quantified spatial uncertainty. *SOIL* **7**, 217–240 (2021).
92. He, X. et al. Global patterns and drivers of soil total phosphorus concentration. *Earth Syst. Sci. Data* **13**, 5831–5846 (2021).
93. Bagozzi, R. P. & Yi, Y. Specification, evaluation, and interpretation of structural equation models. *J. Acad. Market. Sci.* **40**, 8–34 (2012).
94. Li, Y. Global ecosystem iso/anisohydry estimates based on QuikSCAT backscatter and AMSR-E VOD. *figshare* https://doi.org/10.6084/m9.figshare.5323987.v1 (2017).

95. He, X. et al. A global dataset of soil total phosphorus concentration in (semi-)natural terrestrial ecosystems. *figshare* https://doi.org/10.6084/m9.figshare.14583375.v9 (2021).
96. Liu, Y. et al. code for 'Drought legacies delay spring green up in northern ecosystems'. *figshare* https://doi.org/10.6084/m9.figshare.26130907 (2025).

Acknowledgements

This study is supported by the National Key R&D Program of China (2023YFF0805702) and the National Natural Science Foundation of China (42141005). Y.L. acknowledges additional support from the National Natural Science Foundation of China (42301016). S.A.K. was supported by the US National Science Foundation Division of Environmental Biology award no. 2331162. J.P. was supported by the Catalan Government grant AGAUR2023 CLIMA 00118. This work is supported by High-performance Computing Platform of Peking University.

Author contributions

Y.Z. conceived the idea. Y.Z. and Y.L. designed the study. Y.L. performed the analysis. Y.L. and Y.Z. prepared the figures and wrote the first draft of the manuscript. All authors contributed to the interpretation of the results and the revisions of the text.

Competing interests

The authors declare no competing interests.

Additional information

Extended data is available for this paper at https://doi.org/10.1038/s41558-025-02273-6.

Supplementary information The online version contains supplementary material available at https://doi.org/10.1038/s41558-025-02273-6.

Correspondence and requests for materials should be addressed to Yao Zhang.

Peer review information *Nature Climate Change* thanks Cyrille Rathgeber and the other, anonymous, reviewer(s) for their contribution to the peer review of this work.

https://doi.org/10.1038/s41558-025-02273-6

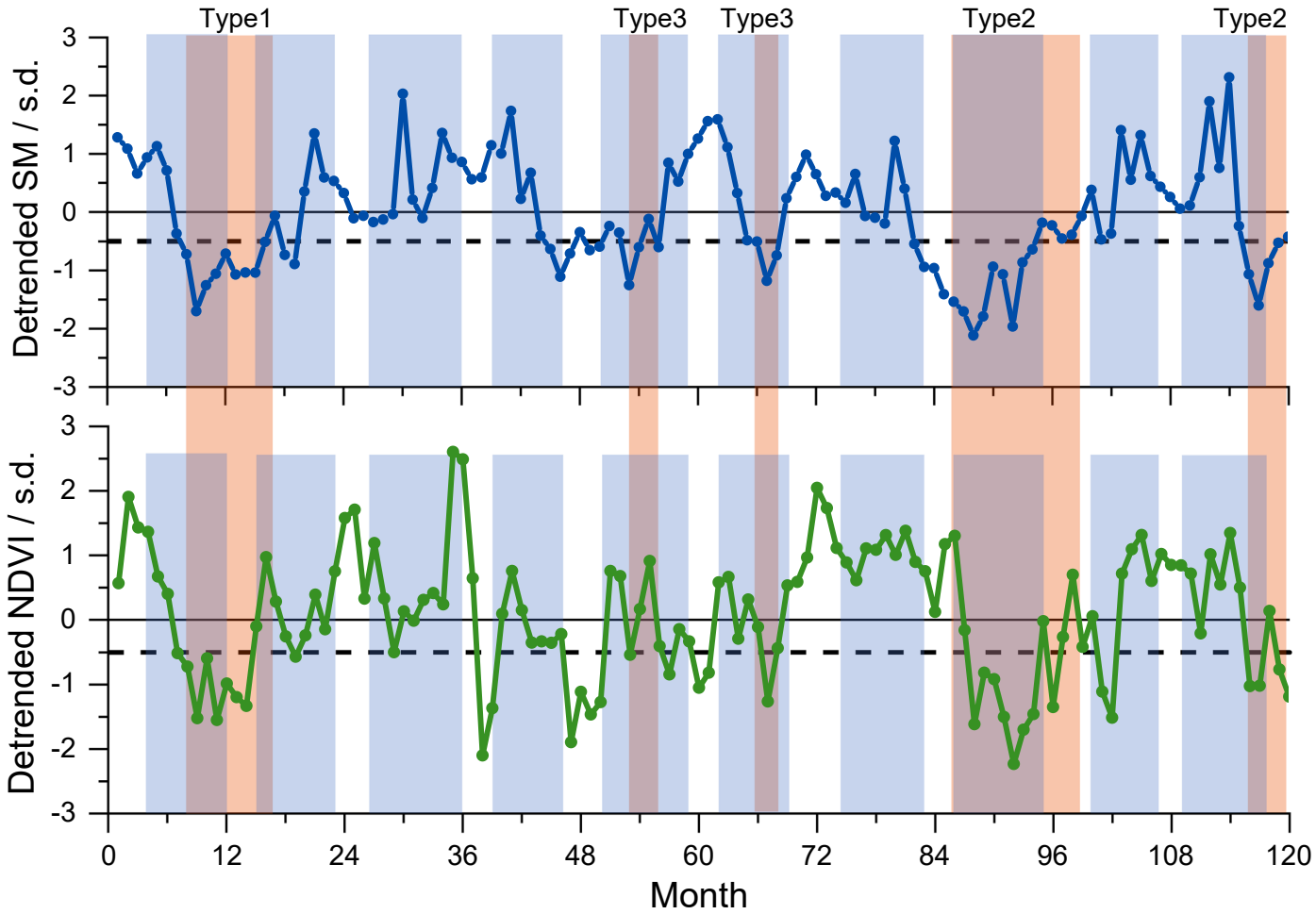

Extended Data Fig. 1 | The schematic diagram of growing season drought identification using soil moisture (SM) and Normalized Difference Vegetation Index (NDVI). A growing season effective drought occurred when deseasonalized soil moisture is below 0.5 s.d. for consecutive two months within growing season, and deseasonalized NDVI is below −0.5 s.d. east one month simultaneously. Type 1 drought: SM has not been recovered before the next growing season. Type 2 drought: SM recovered after the current growing season. Type 3 drought: SM recovered (SM anomaly higher than 0) within the current growing season. The blue background indicates the growing season, and the red background represents drought events.

https://doi.org/10.1038/s41558-025-02273-6

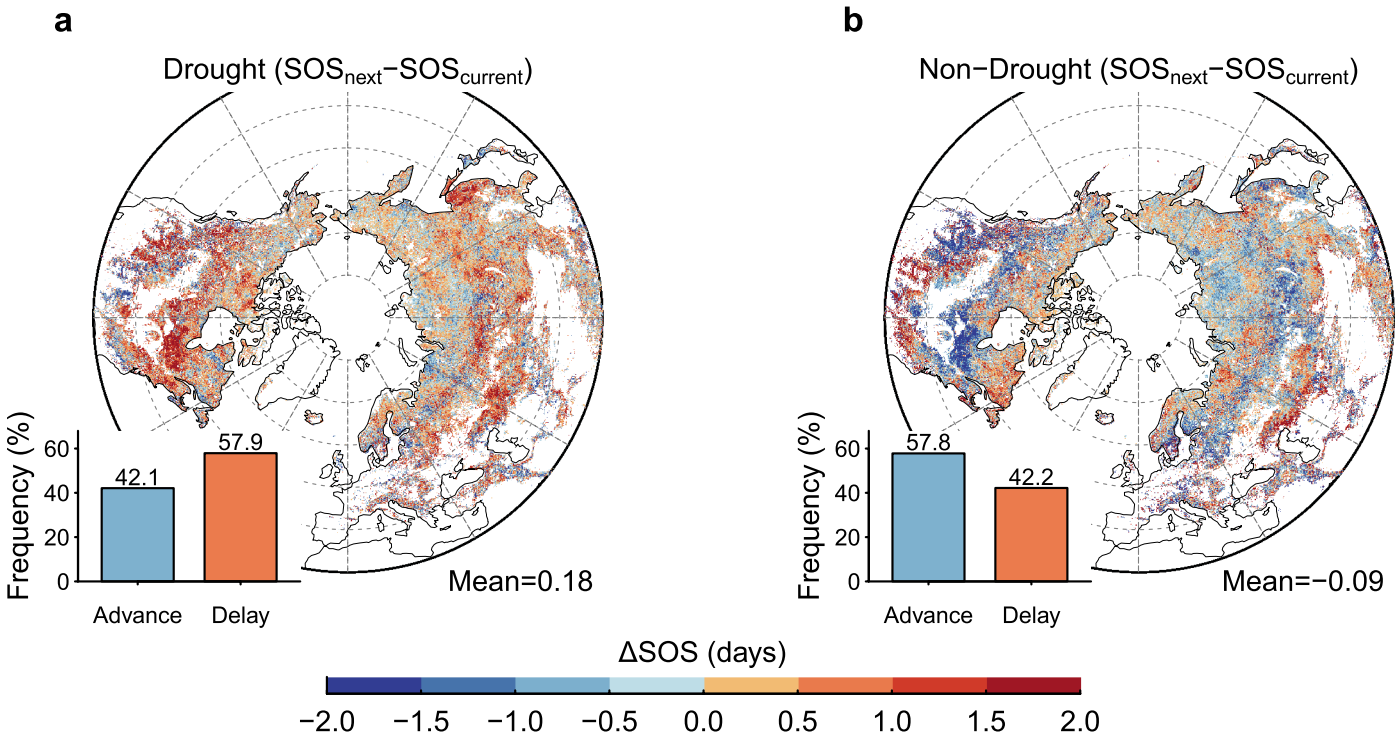

Extended Data Fig. 2 | The long-term effects of drought on the start of growing season (SOS) during 1982-2015. Spatial distribution of cumulative changes between next year's SOS (SOS_{next}) and current year's SOS ($SOS_{current}$), normalized by the average over 34 years, when droughts occurred (**a**) and not occurred (**b**). Insets show the area fraction of SOS delayed (orange) or advanced (blue) by drought.

https://doi.org/10.1038/s41558-025-02273-6

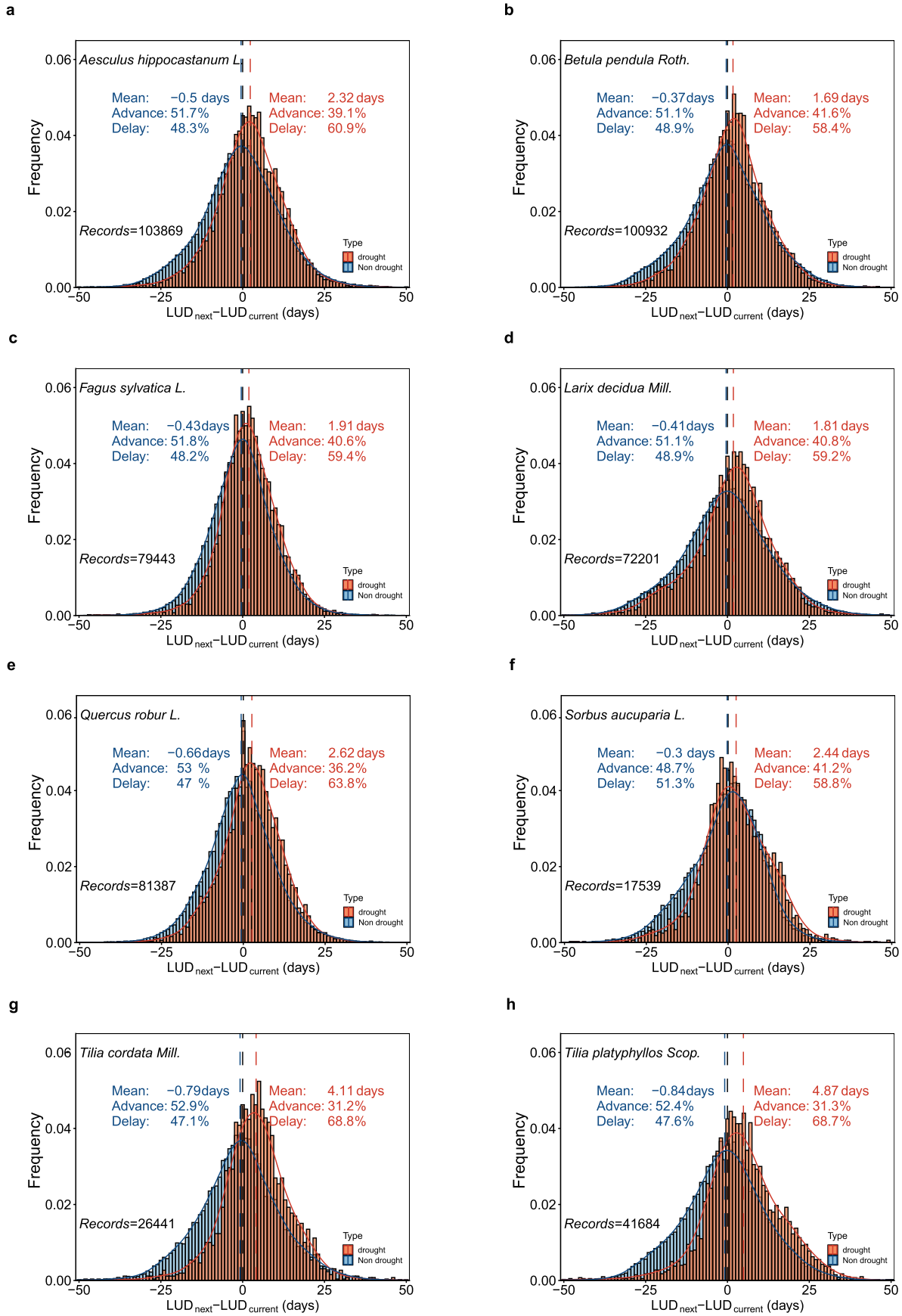

Extended Data Fig. 3 | Effects of drought on next year's leaf unfolding date (LUD) using ground-based observations of eight species. Changes in $LUD_{next} - LUD_{current}$ when drought occurred or not for *Aesculus hippocastanum* L. (**a**), *Betula pendula* Roth (**b**), *Fagus sylvatica* L. (**c**), *Larix decidua* Mill. (**d**), *Quercus robur* L. (**e**), *Sorbus aucuparia* L. (**f**), *Tilia cordata* Mill. (**g**) and *Tilia platyphyllos* Scop. (**h**).

https://doi.org/10.1038/s41558-025-02273-6

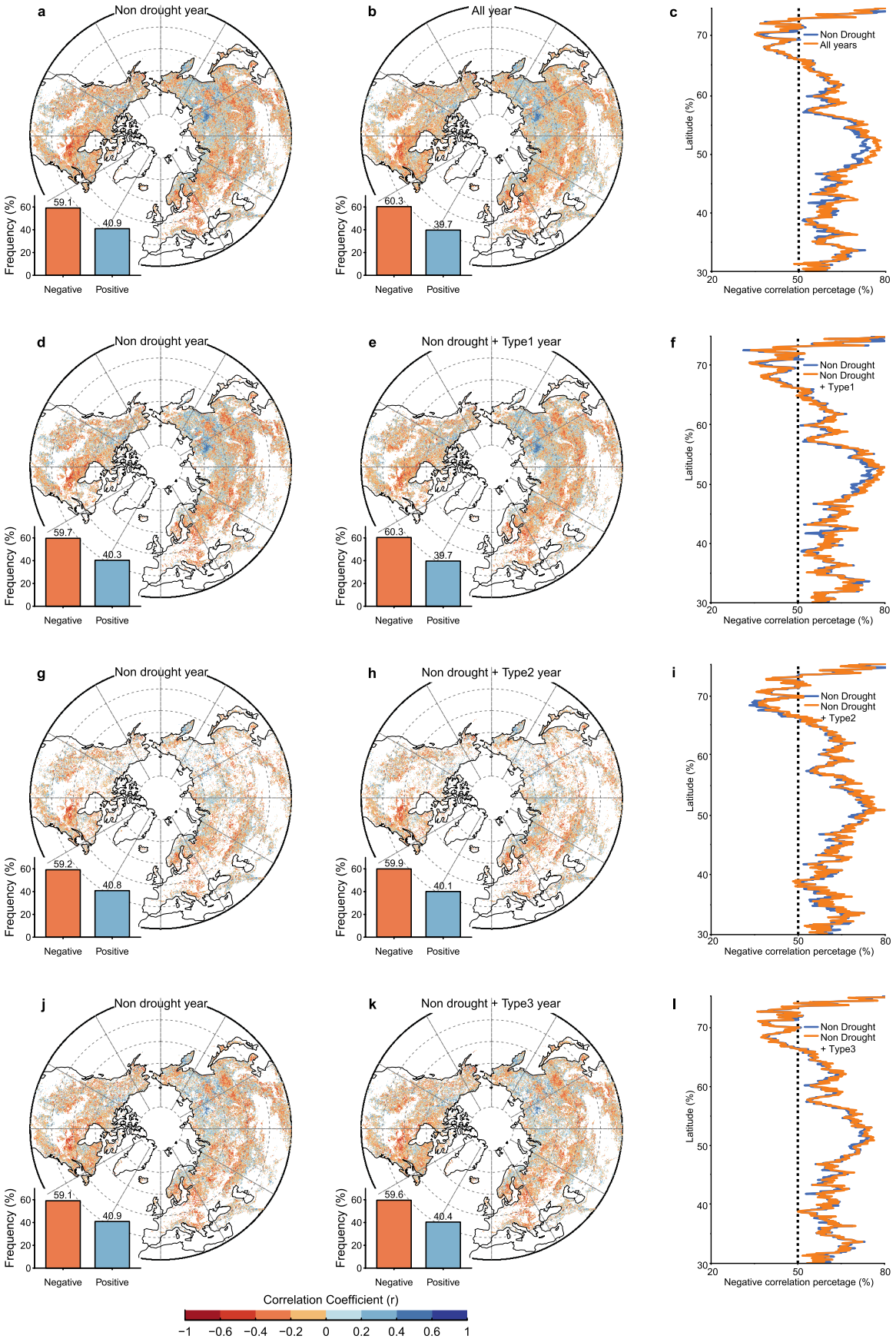

Extended Data Fig. 4 | The spatial patterns of the correlation between current year's EOS and next year's SOS. The results for non-drought years (**a**, **d**, **g**, **j**), all years (**b**), Type 1 and non-drought years (**e**), Type 2 and non-drought years (**h**), Type 3 and non-drought years (**k**). The percentage of negative correlation between EOS and next year's SOS along latitudes (**c**, **f**, **i** and **l**).

https://doi.org/10.1038/s41558-025-02273-6

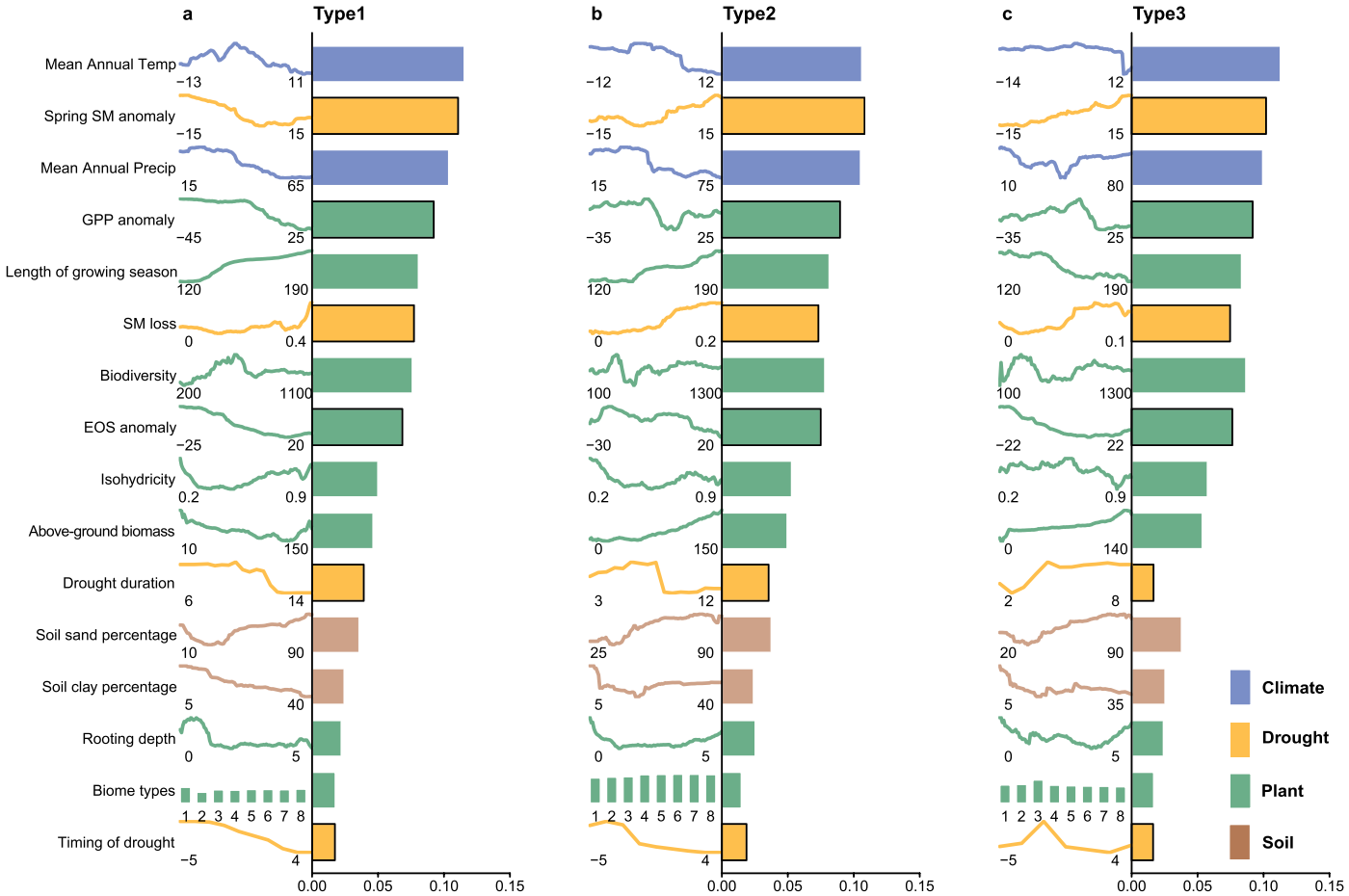

Extended Data Fig. 5 | Response functions for start of the growing season (SOS) changes (SOS_{obs}–SOS_{pred}) following three types of droughts. Results from three random forest models for Type 1 (**a**), Type 2 (**b**), and Type 3 (**c**) droughts. Left panels show response functions with lower and upper bounds of independent variables. Bars on the right indicate variable importance. Blue denotes climatic factors, yellow represents drought characteristics, green shows biological variables, and red indicates soil composition variables. Variables with black borders are time-varying for each drought event; others are static. Code for biome types 1. Temperate Broadleaf and Mixed Forests; 2. Temperate Coniferous Forests; 3. Boreal Forests/Taiga; 4. Temperate Grasslands, Savannas, and shrublands; 5. Montane Grasslands and shrublands; 6. Tundra; 7. Mediterranean Forests; 8. Xeric shrublands.

https://doi.org/10.1038/s41558-025-02273-6

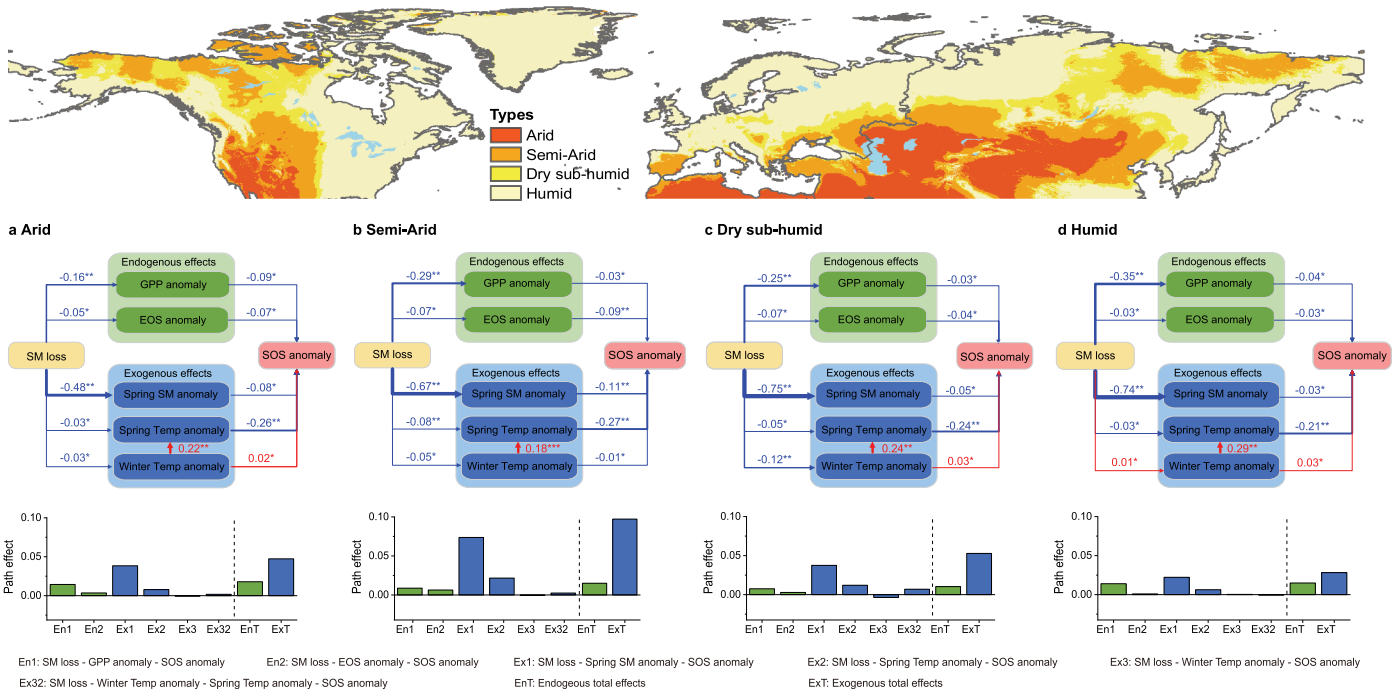

Extended Data Fig. 6 | The path diagrams and path effects of the underlying mechanisms for the relationship between the soil moisture loss (SM_{loss}) and the anomaly of the start of the growing season (SOS) for different arid types. **a-d**, The results for arid (**a**), semi-arid (**b**), dry sub-humid (**c**) and humid (**d**) regions. The numbers represent the mean of standardized path coefficients, with asterisks denote the significance (**P < 0.01; *P < 0.05). The colors and widths of the arrows represent the signs (blue for negative, red for positive) and magnitudes of the path coefficients, respectively. The significance was based on a two-tailed Student's t-test. En1, En2, Ex1, Ex2, Ex3, Ex32 indicate the effect of six major paths; EnT is the total endogenous effect, and ExT is the total exogenous effect.

https://doi.org/10.1038/s41558-025-02273-6

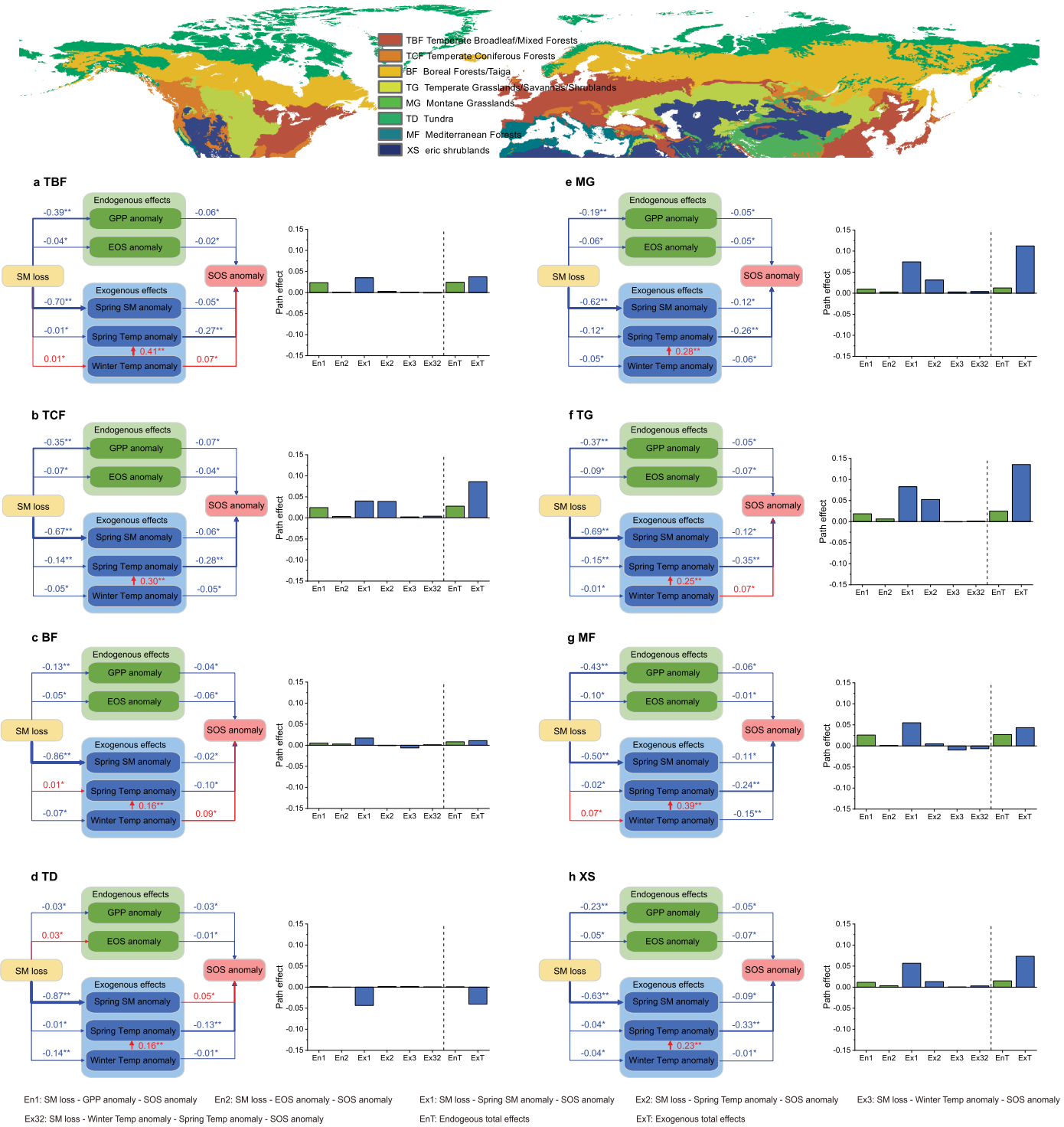

Extended Data Fig. 7 | The path diagrams and path effects of the underlying mechanisms for the relationship between the soil moisture loss (SM_{loss}) and the anomaly of the start of the growing season (SOS) for eight biomes. **a-h**, The results for temperate broadleaf and mixed forests (**a**), temperate coniferous forests (**b**), boreal forests/taiga (**c**), tundra (**d**), montane grasslands and shrublands (**e**), temperate grasslands, savannas and shrublands (**f**), Mediterranean forests (**g**) and xeric shrublands (**h**). The numbers represent the mean of standardized path coefficients, with asterisks denote the significance (**P < 0.01; *P < 0.05). The colors and widths of the arrows represent the signs (blue for negative, red for positive) and magnitudes of the path coefficients, respectively. The significance was based on a two-tailed Student's t-test. En1, En2, Ex1, Ex2, Ex3, Ex32 indicate the effect of six major paths; EnT is the total endogenous effect, and ExT is the total exogenous effect.

https://doi.org/10.1038/s41558-025-02273-6

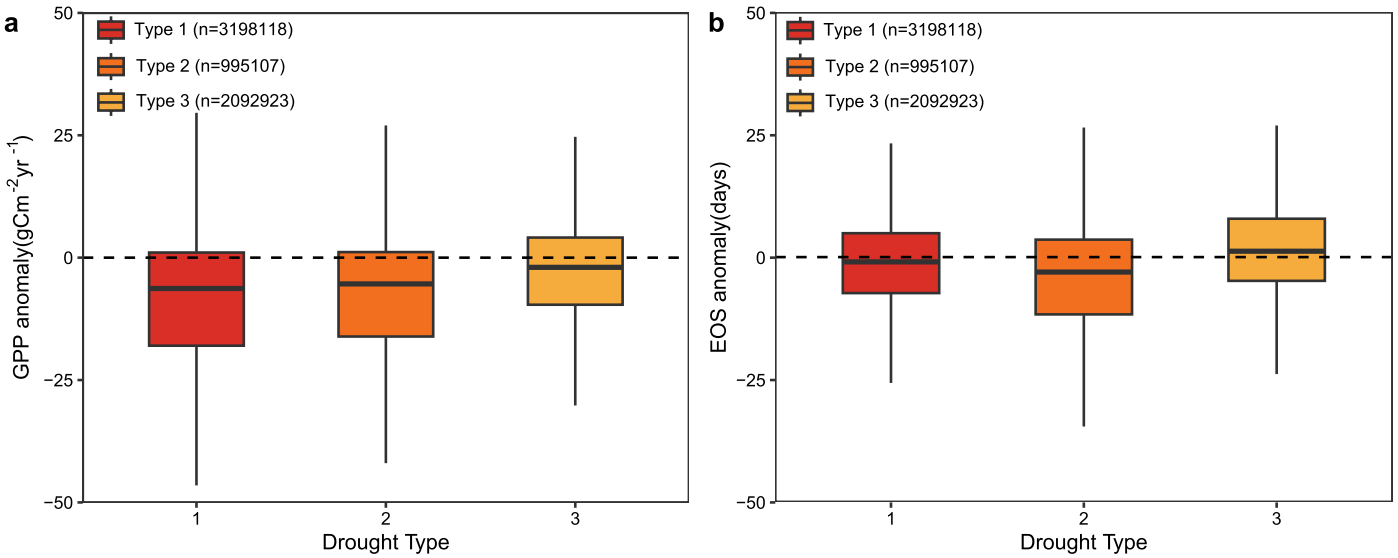

Extended Data Fig. 8 | The anomaly of GPP and EOS of drought years across three drought types. The GPP (**a**) and EOS (**b**) anomalies of drought years compared to the multi-year average. Length of each box indicates the interquartile range, the horizontal line inside each box the median, and the bottom and top of the box the first and third quartiles, respectively.

https://doi.org/10.1038/s41558-025-02273-6

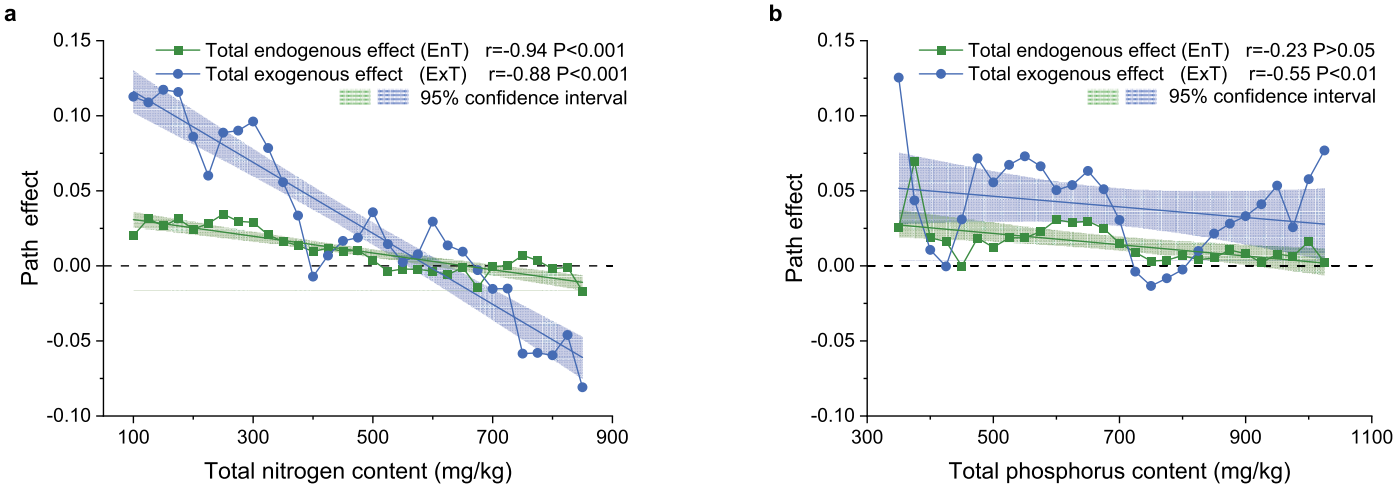

Extended Data Fig. 9 | The legacy effect of drought along soil nutrient gradient. The total endogenous effect and total exogenous effect of drought along soil nitrogen content (**a**) and soil phosphorus content (**b**) at 0-30 cm depth. Each dot represents the average path effect for regions within each bin along nitrogen content or phosphorous content. Shades represent the 95% confidence interval.

nature portfolio

Corresponding author(s): Yao Zhang

Last updated by author(s): Dec 7, 2024

Reporting Summary

Nature Portfolio wishes to improve the reproducibility of the work that we publish. This form provides structure for consistency and transparency in reporting. For further information on Nature Portfolio policies, see our Editorial Policies and the Editorial Policy Checklist.

Statistics

For all statistical analyses, confirm that the following items are present in the figure legend, table legend, main text, or Methods section.

n/a	Confirmed
☐	☒ The exact sample size (*n*) for each experimental group/condition, given as a discrete number and unit of measurement
☐	☒ A statement on whether measurements were taken from distinct samples or whether the same sample was measured repeatedly
☐	☒ The statistical test(s) used AND whether they are one- or two-sided *Only common tests should be described solely by name; describe more complex techniques in the Methods section.*
☐	☒ A description of all covariates tested
☒	☐ A description of any assumptions or corrections, such as tests of normality and adjustment for multiple comparisons
☐	☒ A full description of the statistical parameters including central tendency (e.g. means) or other basic estimates (e.g. regression coefficient) AND variation (e.g. standard deviation) or associated estimates of uncertainty (e.g. confidence intervals)
☐	☒ For null hypothesis testing, the test statistic (e.g. *F*, *t*, *r*) with confidence intervals, effect sizes, degrees of freedom and *P* value noted *Give P values as exact values whenever suitable.*
☒	☐ For Bayesian analysis, information on the choice of priors and Markov chain Monte Carlo settings
☒	☐ For hierarchical and complex designs, identification of the appropriate level for tests and full reporting of outcomes
☐	☒ Estimates of effect sizes (e.g. Cohen's *d*, Pearson's *r*), indicating how they were calculated

Our web collection on statistics for biologists contains articles on many of the points above.

Software and code

Policy information about availability of computer code

Data collection	Data collection is performed in Matlab R2022a.
Data analysis	Data analysis is performed in Matlab R2022a , R 4.1.3 and Python 3.10.9.

For manuscripts utilizing custom algorithms or software that are central to the research but not yet described in published literature, software must be made available to editors and reviewers. We strongly encourage code deposition in a community repository (e.g. GitHub). See the Nature Portfolio guidelines for submitting code & software for further information.

Data

Policy information about availability of data

All manuscripts must include a data availability statement. This statement should provide the following information, where applicable:

- Accession codes, unique identifiers, or web links for publicly available datasets
- A description of any restrictions on data availability
- For clinical datasets or third party data, please ensure that the statement adheres to our policy

The data that support the findings of this study are derived from the following resources. The PEP725 dataset can be downloaded from www.pep725.eu, the RCNN dataset can be downloaded from https://doi.org/10.1038/s41597-020-0376-z, the CPON dataset can be downloaded from http://www.cpon.ac.cn/. The GIMMS NDVI 3g v1 is available at http://poles.tpdc.ac.cn/en/data/9775f2b4-7370-4e5e-a537-3482c9a83d88/. The soil moisture data are available at https://www.gleam.eu/. The SPEI dataset is available at https://spei.csic.es/database.html. The CRU climate dataset is available at https://crudata.uea.ac.uk/cru/data/hrg/.

FLUXCOM GPP dataset can be downloaded from https://www.fluxcom.org/. The maximum root depth data is available at https://wci.earth2observe.eu/thredds/catalog/usc/root-depth/catalog.html, the plant biodiversity data is available at http://ecotope.org/anthromes/biodiversity/plants/data/, mean above-ground biomass data is available at https://daac.ornl.gov/cgibin/dsviewer.pl?ds_id=1763, iso/anisohydry data is available at https://figshare.com/projects/Estimating_global_ecosystem_iso_anisohydry_using_active_an d_passive_microwave_satellite_data/19492, the biomes data can be downloaded from https://www.worldwildlife.org/publications/terrestrial-ecoregions-of-the-world, the land cover data is available at https://lpdaac.usgs.gov/products/mcd12q1v006/, the soil properties data can be downloaded from https://daac.ornl.gov/SOILS/guides/HWSD.html.

Human research participants

Policy information about studies involving human research participants and Sex and Gender in Research.

Reporting on sex and gender	N/A
Population characteristics	N/A
Recruitment	N/A
Ethics oversight	N/A

Note that full information on the approval of the study protocol must also be provided in the manuscript.

Field-specific reporting

Please select the one below that is the best fit for your research. If you are not sure, read the appropriate sections before making your selection.

☐ Life sciences ☐ Behavioural & social sciences ☒ Ecological, evolutionary & environmental sciences

For a reference copy of the document with all sections, see nature.com/documents/nr-reporting-summary-flat.pdf

Ecological, evolutionary & environmental sciences study design

All studies must disclose on these points even when the disclosure is negative.

Study description	Global warming has increased the frequency and intensity of droughts, but the extent to which drought legacy effects influence plant phenology the following year remains unclear. Using long-term satellite observations and ground phenological records, together with state-of-the-art phenology models, we first investigated the impact of drought events on the subsequent year's green-up in northern ecosystems. By utilizing random forest algorithms and path analysis, we further explored the underlying mechanisms of drought legacies on the subsequent year's green-up, and examined both exogenous and endogenous memory effects.
Research sample	This study covers both satellite observation samples and long-term in situ phenological observation samples.
Sampling strategy	We used as many ground samples with long-term high quality phenological records as possible.
Data collection	Ying Liu collected the data required for this study, and the details of the data availability are provided in the main text.
Timing and spatial scale	We used both satellite observations (1982-2015) across mid- and high-latitudinal Northern Hemisphere (30°N), and long-term in situ observations (since 1901) from Europe(1945-2016), Russia (1901-2017) and China (1962--2014).
Data exclusions	For ground phenology records, we excluded sites with less than 5 years of consecutive records.
Reproducibility	We provide all the detailed methods and data sources, programming code and results in both the manuscript and supplementary information files to ensure the reproducibility of this work.
Randomization	This is not relevant to our study because our work is not an Experimental study.
Blinding	Blinding is not relevant to this study, because this study only uses published datasets.

Did the study involve field work? ☐ Yes ☒ No

Reporting for specific materials, systems and methods

We require information from authors about some types of materials, experimental systems and methods used in many studies. Here, indicate whether each material, system or method listed is relevant to your study. If you are not sure if a list item applies to your research, read the appropriate section before selecting a response.

Materials & experimental systems

n/a	Involved in the study
☒	☐ Antibodies
☒	☐ Eukaryotic cell lines
☒	☐ Palaeontology and archaeology
☒	☐ Animals and other organisms
☒	☐ Clinical data
☒	☐ Dual use research of concern

Methods

n/a	Involved in the study
☒	☐ ChIP-seq
☒	☐ Flow cytometry
☒	☐ MRI-based neuroimaging